Composition and Vertical Flux of Particulate Organic Matter to the Oxygen Minimum Zone of the Central Baltic Sea: Impact of a sporadic North Sea inflow

Carolina Cisternas-Novoa*, Frédéric A.C. Le Moigne, Anja Engel.

GEOMAR, Helmholtz Centre for Ocean Research Kiel, Düsternbrooker Weg 20, D-24105 Kiel

**Corresponding author:* Carolina Cisternas-Novoa, GEOMAR, Helmholtz Centre for Ocean Research Kiel, Düsternbrooker Weg 20, D-24105 Kiel, Germany, +49 431 600-4146 ccisternas@geomar.de

Keywords: Baltic Sea, Oxygen minimum zone, POC, PN, POP, TEP, CSP, Sediment trap, Export efficiency.

Abstract

Sinking particles are the main form to transport photosynthetically fixed carbon from the euphotic zone to the ocean interior via the biological carbon pump (BCP). Oxygen (O_2) depletion may improve the efficiency of the BCP. However, how the lack of O_2 mechanistically enhances particulate organic matter (POM) fluxes is not well understood. Here, we investigate distributions and fluxes of POM in two deep basins in the Baltic Sea (GB: Gotland basin and LD: Landsort Deep) with contrasting oxygenation regimes, resulting from a major oxygen-rich saltwater inflow event that oxygenated the bottom waters of GB but not the LD. In June 2015, we deployed surface tethered sediment traps in oxygenated surface waters (GB:40 and 60 m; LD: 40 and 55m), within the oxygen minimum zone (OMZ, GB: 110 m and LD: 110 and 180 m), and at deeper waters oxygenated by the inflow in GB (180 m). We hypothesize that the different O_2 conditions in the water column of the GB compared with the LD affected the POM distribution and caused differences in export efficiency between those two stations.

Fluxes and composition of sinking particles were different in the GB and the LD. In the GB, POC flux was 18% lower in the shallowest trap (40 m) than in the deepest sediment trap (at 180 m). Particulate nitrogen (PN) and Coomassie stainable particles (CSP) fluxes decreased with depth, and particulate organic phosphorus (POP), biogenic silicate (BSi), Chl *a*, and transparent exopolymeric particles (TEP) clearly peaked within the core of the oxygen minimum zone (OMZ, 110 m); this coincided with a high flux of manganese oxide (MnOx)-like particles. In the LD, POC, PN, and CSP fluxes decreased 28, 42 and 56% respectively from the surface to deep waters. POP, BSi and TEP fluxes, however, did not decrease with depth and were slightly higher in the 110 m sample. During this study, MnOx-like particle flux was two orders of magnitude higher in the GB (affected by the 2014/2015 North Sea inflow) relative to the LD.

Our results suggest that MnOx-like particles, formed after the inflow of oxygenated water into the GB, may form aggregates containing, not only transparent exopolymeric particles, as indicated previously, but also POC, POP, BSi, and Chl *a*. Aggregates composed of MnOx-like particles and POM may accumulate in the redoxcline, where they formed larger particles that eventually sink to

the seafloor. We propose that this mechanism would alter the vertical distribution and the flux of POM, and it may contribute to the higher transfer efficiency of POC in the GB. This idea is consistent with the fact that the OM reaching the seafloor was fresher and less degraded in the GB than in the LD.

1. Introduction

Sinking particles are the primary vehicles for transporting photosynthetically fixed carbon from the surface to the deep ocean via the BCP (Boyd and Trull, 2007; Turner, 2015). It has been suggested that the transfer of particulate organic carbon (POC) from the euphotic zone to the ocean interior is enhanced in oxygen minimum zones (OMZs) (Cavan et al., 2017; Devol and Hartnett, 2001; Engel et al., 2017; Keil et al., 2016; van Mooy et al., 2002). Possible mechanisms explaining the higher POC transfer include: i) the reduction of aggregate fragmentation due to the lower zooplankton abundance within the OMZ (Cavan et al., 2017; Keil et al., 2016); ii) a higher refractory nature of sinking particles (Keil et al., 2016; van Mooy et al., 2002); iii) a decrease in heterotrophic microbial activity due to oxygen limitation (Devol and Hartnett, 2001); iv) the preferential degradation of nitrogen-rich organic compounds (Kalvelage et al. 2013; Van Mooy et al. 2002, Engel et al. 2017), and v) changes in ballast materials that may alter the sinking velocity and protect organic matter from degradation (Armstrong et al., 2002). However, mechanisms of how low O_2 concentration would affect the composition and fate of sinking OM, and the efficiency of the biologic carbon pump in oxygen-deficient basins have hardly been investigated.

The semi-enclosed, brackish Baltic Sea is a unique environment with strong natural gradients of salinity and temperature (Kullenberg and Jacobsen, 1981), primary productivity, nutrients (Andersen et al., 2017), and O_2 concentrations (Carstensen et al., 2014a). New production, defined as the fraction of the autotrophic production supported by allochthonous sources of nitrogen (Dugdale and Goering, 1967) is considered equivalent to the particulate OM export (Eppley and Peterson, 1979; Legendre and Gosselin, 1989) on appropriate timescales. In the Baltic Sea, new production varies seasonally (Thomas and Schneider, 1999); spring and summer are periods of elevated new production supported by the diatom-dominated spring bloom and by

diazotrophic cyanobacteria, respectively (Wasmund and Uhlig, 2003). Based on sediment trap data, collected at 140 m depth in the Gotland Basin, Struck et al. (2004) reported that the highest fluxes of POC occur in fall, followed by summer and spring. Using $\delta^{15}N$ they showed that during the summer, N_2 fixation by diazotrophic species was the primary source (~41%) of the exported nitrogen, and that the majority of the particulate OM sedimenting in the central Baltic Sea is of pelagic origin.

OM export from the euphotic zone to the seafloor has a dual significance in the deep basins of the Baltic Sea. On the one hand, it contributes to the long-term burial of POC, and consequently to the removal and long-term storage of CO_2 from surface waters (Emeis et al., 2000; Leipe et al., 2011); on the other hand, it connects the pelagic and the benthic systems contributing to the oxygen consumption and hence deoxygenation at depth. Environmental and anthropogenic changes may alter the magnitude and composition of OM transferred from the surface to the seafloor in the Baltic Sea (Tamelander et al. 2017). The reduction of nutrient inputs as targeted by the Baltic Marine Environment Protection Commission (HELCOM) can cause a decrease in OM downward flux and limit the oxygen depletion. However, to fully suppress hypoxia enhanced ventilation would be necessary the bottom waters of the Baltic Sea.

The Gotland Basin (GB), and the Landsort Deep (LD) are the deepest basins of the Baltic Sea. They exhibit permanent bottom-water hypoxia (Conley et al. 2002), caused by a combination of limited water exchange with the North Sea through the Kattegat Strait, strong vertical stratification, and high production /remineralization of OM due to eutrophication (Carstensen et al., 2014b; Conley et al., 2009). From the1950s to 1970s, the hypoxic zones (<60 µmol O_2 kg^{-1}) in the Baltic Sea had expanded fourfold (Carstensen et al. 2014). Salt-water inflows from the North Sea are the primary mechanism renewing deep water in the central Baltic Sea. A Major Baltic Inflow (MBI) occurred in 2014/2015 (Mohrholz et al. 2015); this event ventilated bottom waters for five months between February and July 2015 (Holtermann et al., 2017). The 2014/2015 MBI caused the intrusion of O_2 to deep hypoxic waters, a substantial temperature variability (Holtermann et al., 2017), the displacement of remnant stagnant water masses by new water that

changed the chemistry of the water column (Myllykangas et al., 2017), and high turbidities that may be associated with redox reactions products (Schmale et al., 2016). At the time of sampling (June 2015), this MBI had reached the Gotland Basin , but did not affect the LD, located further northwest. In the LD, water properties did not change due to the MBI, the sulfidic layer was maintained (hydrogen sulfide, H_2S concentrations of 20.7- 21.2 μM), and salinity varied between 10.6 and 10.9 (Holtermann et al., 2017).

In the GB and the LD, a permanent transition zone of about 2 to 10 m thickness separates the surface oxygenated and the oxygen-deficient waters; the approximated position of the pelagic redoxcline is between 127 and 129 m in the GB and between 79 and 85 m in the LD (Glockzin et al., 2014). The water column stratification is only disrupted by sporadic intrusions of saline, well-oxygenated waters from the North Sea (Günter et al., 2008). In the GB, the 2014/2015 MBI oxygenated the deep water column, removed the sulfidic waters in the deeper layers below the redoxcline, and created a secondary near-bottom redoxcline (Schmale et al., 2016). A steep redox gradient characterizes the pelagic redoxcline; here electron acceptors and their reduced counterparts are vertically segregated, and biogeochemical transformations mediated by microbial processes are actively occurring (Bonaglia et al., 2016; Brettar and Rheinheimer, 1991; Neretin et al., 2003). For instance, iron (Fe) and manganese (Mn) undergo rapidly reversible transformations at the redox interface. Under anoxic conditions, these metals are present in dissolved reduced forms Mn(II) and Fe(II); under oxic conditions or in presence of nitrate they react with O_2 and form particulate oxides. Manganese oxides (MnOx) production may be microbially mediated (Neretin et al., 2003; Richardson et al., 1988), or authigenic (Glockzin et al., 2014). The reduction of Mn(IV) with sulfide occurs within a scale of seconds to minutes (Neretin et al., 2003), and is inhibited by nitrate (Dollhopf et al., 2000). The sporadic oxygenation of the deep water of the GB combined with the release of Mn from the sediments into the water column (Lenz et al., 2015) generate appropriate conditions for particulate MnOx formation. MnOx particles have previously been observed in pelagic redoxclines in the Baltic Sea (Glockzin et al., 2014; Neretin et al., 2003). They are amorphous or star-shaped particles that can occur as single particles or form aggregates

123 enriched in OM (Neretin et al., 2003), specifically with transparent exopolymer particles (TEP)
124 (Glockzin et al., 2014). TEP are highly sticky, polysaccharide-rich particles that can enhance
125 aggregation and the formation of marine snow (Engel, 2000; Logan et al., 1995). Thus, MnOx-
126 OM aggregates may significantly contribute to the downward flux of POC. However, TEP are
127 less dense than seawater (Azetsu-Scott and Passow, 2004); therefore they could also reduce the
128 density of marine aggregates and decrease their sinking velocity if the ratio of dense particles to
129 TEP is too small (Azetsu-Scott and Passow, 2004; Engel and Schartau, 1999; Mari et al., 2017).
130 Mixed aggregates containing MnOx and TEP have reported before for the GB and LD (Dellwig et
131 al. 2010; Glockzin et al. 2014). Their sizes ranged between 0.8 and 41 μm equivalent spherical
132 diameter (ESD), and their sinking velocity (0.76 m d^{-1}) was lower than what was predicted by the
133 Stokes' law (Glockzin et al., 2014) possibly due to their star-shaped morphology and the high OM
134 content attached to them. Additionally, MnOx aggregates may affect the cycling of particle-
135 reactive elements like phosphorus and trace metals via scavenging processes (Dellwig et al.,
136 2010). To date, there are no measurements of the density of MnOx-OM aggregates, their potential
137 ballast effect of sinking OM, or their effect on the flux of particle-reactive elements in the Baltic
138 Sea.

139 The objectives of this study are, first, to characterize the amount and composition of particles
140 sinking out of the euphotic zone in two deep basins of the Baltic Sea: the GB and the LD. Second,
141 to study how the oxygenation of deep waters (below 140 m) in the GB caused by the 2014/2015
142 MBI will affect the sinking fluxes of POM compared with LD that was not affected by the MBI
143 and exhibited low O_2 concentration (below 74 m) and sulfidic conditions (below 160 m) in the
144 deep water. We hypothesize that the MBI that altered the water column chemistry and created
145 different O_2 conditions in the GB compared with the LD affected the abundance and *in-situ*
146 formation of MnOx rich-aggregates and subsequently OM distribution causing differences in
147 degradation and export of OM between those two stations.

148 **2. Methods**

149 *2.1. Sampling location and water column properties*

Samples were collected during the BalticOM cruise in the Baltic Sea onboard the *RV Alkor* form June 3th to June 19th, 2015. We collected sinking particles using surface-tethered sediment traps (Engel et al., 2017; Knauer et al., 1979) in the GB and the LD (Fig.1). Additionally, water column samples (table 2) were collected using a Niskin-bottle rosette at the locations of the trap deployments. Temperature, salinity and O_2 concentration were determined at each station using a Sea-Bird (CTD) probe equipped with a oxygen (Oxyguard, PreSens), calibrated with discrete samples measured using the Winkler method (Strickland and Parsons, 1968; Wilhelm, 1888).

2.2. Sediment trap design and deployment

We deployed two surface-tethered sediment traps for two days in the GB, and one day in the LD (Fig.1). Each trap collected particles at four depths 40, 60 (55 in LD), 110 and 180 m (Table 1) to estimate POM fluxes to and within the OMZ. The sediment trap consisted of five (two traps were located at 40 m in each station to evaluate replicability) arrays of 12 acrylic particle interceptor tubes (PITs) mounted in a PVC cross frame; each tube was equipped with an acrylic baffle at the top to minimize the collection of swimmers (Engel et al., 2017; Knauer et al., 1979). The PITs were 7 cm in diameter and 53 cm in height with an aspect ratio of 7.5 and a collection area of 0.0038 m^{-2}. The cross frame and PITs were attached to a line that had a bottom weight and a set of surface and subsurface floats. The procedures for PIT preparation and sample recovery followed Engel et al. (2017). Shortly before deployment, each PIT was filled with 1.5 L of seawater previously filtered through a 0.2 μm pore size cartridge. A preservative solution of saline brine (50 g L^{-1}) was added slowly to each PIT underneath the 1.5 L of filtered seawater, carefully keeping the density gradient. The PITs were kept covered until deployment and immediately after recovery to avoid contamination. After recovery, the density gradient was visually verified, and the supernatant seawater was siphoned off the PIT. Then, the remaining bottom waters (approx. 0.6 L) containing the particles were pooled together and filled-up to 10 L with filtered seawater. After that, the samples were screened with a 500 μm mesh to remove swimmers. Subsequently, samples were split into aliquots that were processed for the different biogeochemical analysis as described in Engel et al. (2017).

177 *2.3. Biogeochemical analysis*

178 Nutrients were measured in seawater samples of the deployment stations. Ammonium (detection
179 limit 0.05 µM) was measured directly on unfiltered seawater samples on board after Solórzano
180 (1969). Phosphate, nitrate, and nitrite (detection limit 0.04 µM) were filtered through a 0.2 µm
181 pore size and stored frozen until their analysis; samples were measured photometrically with
182 continuous flow analysis on an auto-analyzer (QuAAtro; Seal Analytical) after Grasshoff et al.
183 (1999).

184 Particulate organic carbon (POC), nitrogen (PN), organic phosphorus (POP), and chlorophyll a
185 (Chl *a*) were determined as described in Engel et al. (2017). Aliquots of 100 to 200 ml of the
186 trapped material, and 500 ml for the sampled seawater were filtered in duplicate for each
187 parameter at low vacuum (<200 mbar), onto pre-combusted GF/F filters (8h at 500°C). The filters
188 were stored frozen (-20°C) until analysis. Prior analysis, filters for POC-PN determination were
189 exposed to acid fumes (37% hydrochloric acid) to remove carbonates, and subsequently dried for
190 12h at 60 °C. POC and PN concentrations were determined using an elemental analyzer (Euro
191 EA, Hechatech) after Sharp (1974).

192 POP was analyzed after Hansen and Koroleff (1999). POP was oxidized to orthophosphate by
193 heating the filters in 40 mL of deionized water (18.2MΩ) with Oxisolv (MERCK 112936) for 30
194 min in a pressure cooker. Orthophosphate was determined spectrophotometrically at 882 nm in a
195 Shimadzu UV-VIS Spectrophotometer UV1201.

196 Chl *a* was analyzed after extraction with 10 mL of 90% acetone, the fluorescence of the samples
197 was measured using a Turner fluorimeter (440/685 nm, Turner, 10-AU) according to Strickland et
198 al. (1972). The fluorometer was calibrated with a standard solution of Chl *a* (Sigma-Aldrich C-
199 5753).

200 Phytoplankton composition and abundance in the stations where we deployed sediment traps were
201 evaluated using light microscopy and flow cytometry. Phytoplankton, > 5 µm, was counted and
202 identified in 50 ml of fixed samples (Lugol's solution, 1% final concentration) using a Zeiss
203 Axiovert inverted microscope (200x magnification). The size of the counted phytoplankton

species ranged from 10 to 200 μm. Phytoplankton, <20 μm, cell abundance was quantified using a flow cytometer (FACSCalibur, Becton, Dickson, Oxford, UK). 2 ml samples were fixed with formaldehyde (1% final concentration) and stored frozen (-80 °C) until analysis (two weeks later). Cell counts were determined with CellQuest software (Becton Dickenson); pico- and nanoplankton populations of naturally containing chlorophyll or phycoerythrin (*i.e.*, Synechococcus) were identified and enumerated.

Biogenic silica (BSi) was determined by filtering duplicate aliquots of 50 to 100 mL onto 0.4 μm cellulose acetate filters. Samples were stored at -20°C until analysis. For the measurements, filters were digested in NaOH at 85°C for 135 min; the pH was adjusted to 8 with HCl. Silicate was measured spectrophotometrically according to Hansen and Koroleff (2007).

Transparent exopolymeric particles (TEP) and coomassie stainable particles (CSP) from trap and water column were analyzed by microscopy according to Alldredge et al. (1993) and Long and Azam (1996) respectively. Duplicate aliquots of 5 to 20 ml were filtered onto 0.4 μm Nuclepore membrane filters (Whatmann) and stained with 1 ml of Alcian Blue solution for TEP and Coomassie brilliant blue solution for CSP. Filters were transferred onto Cytoclear ® slides and frozen (-20°C) until microscopy analysis. For the analysis, thirty images for each filter were captured under 200x magnification using a light microscope (Zeiss Axio Scope A.1) connected to a color camera (AxioCam MRc). Particle abundance and area were measured semi-automatically using an image analysis system including the WCIF ImageJ software. The RGB was split in three channels: red, blue and green, and the red was used to quantify the amount of TEP and CSP (Engel 2009). Additionally, TEP and CSP in water samples from the stations where we deployed sediment traps were analyzed spectrophotometrically (with higher vertical resolution than microscopy) according to Passow and Alldredge (1995) and Cisternas-Novoa et al. (2014) respectively. Concentrations of TEP are reported relative to a xanthan gum standard and expressed in micrograms of xanthan gum equivalents per liter (μg XG eq. L^{-1}), and concentrations of CSP are reported relative to a bovine serum albumin standard and expressed in micrograms of bovine serum albumin equivalents per liter (μg BSA eq L^{-1}).

231 The abundance of MnOx-like particle was determined by image analysis, using the same images
232 that for TEP and CSP analysis and a modified version of the method described above. Thirty
233 images per filter (200x) were analyzed semi-automatically using Image J. The blue channel was
234 used to quantify the amount of MnOx-like particles in the water column and sediment traps, in
235 this manner, the MnOx-like particles were clearly visible with a negligible disruption from TEP
236 or CSP stained blue.
237 Total amino acids (TAA) were analyzed in unfiltered seawater and trapped material. Samples
238 were stored at -20°C until analysis. Duplicate samples were hydrolyzed at 100 °C in 6N HCl
239 (Suprapur® Hydrochloric acid 30%) and 11 mM ascorbic acid for 20h. Amino acids were
240 separated and measured by high-performance liquid chromatography (HPLC), after derivatization
241 with ortho-phthaldialdehyde using a fluorescence detector (Excitation/Emission 330/445 nm)
242 (Dittmar et al., 2009; Lindroth and Mopper, 1979). The quantitative degradation index (DI) of
243 Dauwe et al. (1999), based on changes in amino acids composition of the POM as it undergoes to
244 degradation processes in the water column, was calculated using the factor coefficient of Dauwe
245 et al. (1999) and the average and standard deviation of the TAA of this data set.
246 Total combined carbohydrates (TCHO) were determined by ion chromatography according to
247 Engel and Händel (2011). TCHO were analyzed in the unfiltered seawater and sediment trap
248 material. Samples were stored at -20°C until analysis. Prior to analysis, the samples were desalted
249 by membrane dialysis using dialysis tubes with 1 kDa molecular weight cut-off (Spectra Por). The
250 desalination was conducted for 4.5 h at 1°C. Then, a 2 mL subsample was sealed with 1.6 mL 1M
251 HCl in pre-combusted glass ampoules and hydrolyzed. Samples were hydrolyzed for 20 h at
252 100°C. After hydrolysis, the subsamples were neutralized by acid evaporation under N_2
253 atmosphere at 50°C, resuspended with ultrapure Milli-Q water and analyzed by ion
254 chromatography.
255 *2.4 Statistics*
256 Significant differences between two parameters were tested using the Mann-Whitney U-test. The
257 results of statistical analyses were assumed to be significant at *p*-values < 0.05. Statistical
258 analyses were performed using Matlab software (MatlabR2014a).

3. Results

3.1. Biogeochemistry of the water column

The water column of both stations was stratified during the study. In the GB the seasonal thermocline was located between 22 and 37 m, the temperature decreased rapidly from 9.8°C in the surface mix layer to 4.7°C below 37 m. Deeper in the water column, a pycnocline (halocline) coincided with the oxycline and was located between 65 m (S=7.6) and 80 m (S=10.2), below 80 m the salinity gradually increased up to 13.5 at the bottom (220 m). In the GB, a hypoxic layer (<40 μmol O_2 L^{-1}) was located between 74 and 140 m; the core of the OMZ (<10 μmol O_2 L^{-1}) was located between 96 and 125 m. The O_2 concentration increases from 35 μmol O_2 L^{-1} at 140 m to 79 μmol O_2 L^{-1} at 220 m (Fig. 2a). In the LD, the seasonal thermocline was located between 10 and 39 m, where the temperature decreased gradually from 12°C to 4.0°C (Fig. 2b). The pycnocline was between 55 (S=7.2) and 75 m (S=9) below that the salinity is constant (S=10.7) until the bottom of the station (430 m). The O_2 concentration was below the detection limit (<3 μmol O_2 L^{-1}) from 74 m to the bottom.

The vertical profile of nutrients was different at both stations (Fig. 2). In the GB, nitrate concentration increased from below the detection limit, in the upper ten meters, to 0.17 μM at 40 m (Fig. 2a). Concentrations were variable within the OMZ with 6 μM in the upper (80 m) and lower oxycline (140 m), and 0.12 μM in the core of OMZ (110 m); the nitrate concentration decreased to 4.8 μM in the deepest sample (220 m). Nitrite was below the detection limit in most of the water column except for 60 m (0.09 μM) and 110 m (0.11 μM). Ammonium increased from 0.14 μM in upper ten meters to 1.15 μM at 40 m; concentrations were variable in the OMZ with less than 0.15 μM in the upper (80 m) and lower oxycline (140 m), and maximum concentration of 3.28 ± 0.01 μM in the core of the OMZ (110m). Vertical profiles of phosphate and silicate at the GB were similar; the concentrations steadily increased from the upper ten meters of the water column (0.29 μM and 10.36 μM respectively) to the OMZ (2.67 μM and 39.07 μM respectively),

285 and gradually decreased below the OMZ (Fig. 2a). Hydrogen sulfide was not detectable
286 in the GB.
287 In the LD, nitrate and nitrite concentrations were below the detection limit between the surface
288 and 250 m (<0.04 μM) (Fig. 2b). Nitrite showed a maximum of 0.22 μM at 350 m, and nitrate a
289 maximum of 6.0 μM at 400 m. Ammonium concentrations varied between 0.06 and 0.59 μM in
290 the upper 70 m and increased to 5.97 and 8.03 μM in the OMZ (below 74 m). The lowest
291 concentration (0.07μM) was measured in the surface and maximum concentration of 8.03 μM at
292 110 m. Phosphate and silicate concentrations were relatively low within the mixed layer due to
293 phytoplankton consumption; gradually increased below the pycnocline, and decreased between
294 110 and 180 m. Phosphate concentrations varied between 1.5 and 2.5 μM in the upper 110 m of
295 the water column, decreased to 0.22 μM at 180 m and increased to 2.7 μM at 430 m (deepest
296 sample). Silicate ranged between 25 and 38 μM in the upper 110 m of the water column,
297 decreased to 7.4 μM at 180 m, and increased 38.9 μM at 430 m. Hydrogen sulfide was detectable
298 below 180 m, with the highest concentration (3.97 μM) at 250 m and the lowest (0.04 μM)
299 between 300 and 350 m (Fig. 2b).
300 *3.2. Particulate organic matter concentration in the water column*
301 Chl *a* concentration in the upper 10 m was slightly higher in the GB (1.5-1.7 μg L^{-1}, Fig. 3b) than
302 in LD (1.4-1.2 μg L^{-1} and 0.1-0.3 μM, Fig. 3e). In both stations, more than 90% of the total
303 smaller phytoplankton (<20 μm, pico- and nanophytoplankton) abundances, determined by flow
304 cytometry, were measured in the upper 60 m, although phytoplankton was detectable in the entire
305 water column. Pico- and nanophytoplankton abundances were 10% higher in GB than in LD
306 (Table 2). Picocyanobacteria determined by phycoerythrin fluorescence account for 92% and 96%
307 of the total picophytoplankton in GB and LD respectively. Picocyanobacteria was 30% higher in
308 GB than in LD.
309 Large phytoplankton (>5 μm) abundance, determined by microscopy, was 63% higher in the LD
310 than in the GB (Table 3). Filamentous cyanobacteria dominated the large phytoplankton
311 community at both stations with up to 90% corresponding to *Aphanizomenon* sp. Cyanobacteria

312 represented 56% of the total phytoplankton counts in the GB and up to 74% in the LD.
313 Dinoflagellates (dominated by *Dinophysis* sp.) were significant in both stations (19% of the total),
314 whereas chlorophytes (dominated by filaments of *Planctonema* sp. containing cylindrical cells)
315 were more abundant in the GB than in LD (25% and 4% of the total phytoplankton respectively).
316 Diatoms represented less than 1% of the phytoplankton in both stations, and they were slightly
317 more abundant at 40 m in the LD (Table 3). BSi was higher in the upper 10 m (0.4-0.5 μM) and
318 decreased with depth in the GB (Fig. 3b), whereas in the LD, BSi showed a peak at 40 m and then
319 decreased with depth (Fig. 3f).
320 Vertical profiles of POC, PN, and POP concentration were similar in the water column of the two
321 stations (Fig. 3a, d). In the GB, the concentrations were higher in the upper 10 m of the water
322 column (POC: 40.38 ± 0.80, PN: 3.89± 0.01, and POP: 0.26± 0.04 μM) and decreased gradually
323 with depth until 110 m where relatively high concentrations (POC 18 ± 0.63, PN: 2± 0.08, and
324 POP: 0.2 μM) were observed. The lowest concentrations were found at 180 m (POC: 11.97 ±
325 1.03, PN: 1.05± 0.02, and POP <0.03 μM) (Fig. 3a). In the LD, POM decreased with depth from
326 the surface (POC: 35 ± 0.99, PN: 4± 0.09, and POP: 0.2 μM) to 40 m, remained relatively
327 constant between 40 and 80 m and decreased again between 110 and 250 m (Fig. 3d).
328 We observed high concentrations of TEP and CSP in the upper 10 m in both stations. The highest
329 TEP concentration was measured at 1 and 10 m at both stations, and it was slightly higher (19%)
330 in the GB than in the LD (Fig. 3c, f). TEP and CSP vertical profiles were different from each
331 other in the GB (Fig. 3c) and covaried in the LD (Fig. 3f). Like observed for POC, PN, and POP,
332 TEP concentrations showed a peak at 110 m (50.29± 6.17 μg XG eq. L^{-1}) in the GB. The highest
333 concentration of CSP at this station was observed in the shallowest (1 m) sample, CSP
334 concentration decreased quickly below 10 m, and then it increased at 140 and 230 m (the deepest
335 sample ~20 m above the seafloor) (Fig. 3c). In the LD, the highest concentrations of TEP and
336 CSP were measured in surface (1 and 10 m) and at 110 m (Fig. 3f). TEP and CSP decreased with
337 depth in the first 80 m (from 53.26± 7.10 to 18.39± 4.57 μg XG eq. L^{-1} and from 53.26± 7.10 to
338 31.57± 18.78 μg BSA eq. L^{-1}). Both types of gel-like particles showed an increase in

concentration at 110 m (49.25± 4.08 μg XG eq. L^{-1} and 66.89± 22.33 μg BSA eq. L^{-1} respectively). Below 110 m, TEP concentrations stayed relatively constant, while CSP concentrations decreased at 180 m and kept relatively constant below that depth.

3.3. MnOx-like particles vertical distribution in the water column

Dark, star-shaped, MnOx-like particles (Glockzin et al., 2014; Neretin et al., 2003) were only observed below the fully oxygenated mixed layer in the GB and, in less abundance, in the LD (Fig. 4). In GB, single MnOx-like particle and large aggregates were observed from 80 m to 220 m (the deepest sample, approximately 28 m above the seafloor). Relatively high concentration of MnOx-like particles ($2x10^6$ particles L^{-1}), were measured in the upper (80 m) and lower (140 m) oxycline where the O_2 concentration was less than 40 μM, and at 220 m ($4x10^6$ particles L^{-1})(Fig. 4a). The lowest abundance of MnOx-like particles ($7x10^5$ particles L^{-1}) was observed at 110 m, in the core of the OMZ where the O_2 concentration was less than10 μM. The equivalent spherical diameter (ESD) varied between 0.6 and 30.5 μm and the median was 3.0 μm. The largest aggregates were observed in the upper oxycline (80 m). In the LD, MnOx-like particles were less abundant, smaller and had a narrow distribution in the water column than in the GB. MnOx-like particles were not detected in the fully oxic (0-40 m) or fully anoxic (180 to 430 m) water column. At 60 m, right above the oxycline, MnOx-like particles began to appear, however, in relatively low abundance. The maximum abundance, $9x10^5$ particles L^{-1}, was observed in the oxycline at 70 m (Fig. 4b). The ESD varied ranged between 0.6 and 13.4 μm, the largest aggregates were observed at 70 m.

3.4. Fluxes of Particulate Organic Matter

Fluxes of POC and PN varied little with depth in the GB (Fig. 5a-b). POC flux slightly increased (18%) from the shallowest (40 m) to the deepest (180 m) sediment trap. Fluxes of PN and CSP were higher at 40 and 60 m and decreased (19 and 70 %) from 60 to 180 m, respectively (Fig. 5a and 5c). On the other hand, fluxes of POP, BSi, Chl *a* (Fig. 5b) and TEP (Fig. 6a) peaked in the sediment trap located in the core of the OMZ (110 m). The increment of fluxes at 110 m

365 coincided with the presence of abundant MnOx-like particles associated with TEP (Fig. 6a). In
366 addition, TEP size distribution, determined by image analysis, indicated an increase in large TEP
367 at 110 m (data not shown). In contrast, in the LD, POC, PN (Fig. 5d) and CSP (Fig. 6d) fluxes,
368 steadily decreased with depth by 28, 42 and 56% from 40 to 180 m. Similar to the fluxes
369 measured in the GB, the POP, BSi (Fig. 5e) and TEP (Fig. 6c) showed a smaller peak in the
370 sediment trap located at 110 m.
371 MnOx-like particles were drastically less abundant in sediment trap samples from the LD than in
372 the GB and when present, they appear as single particles, not aggregated with TEP or CSP (Fig.
373 6c, d). At both stations, and similar to the water column samples, MnOx-like particles were not
374 observed in sediment trap samples collected, in fully oxygenated depths (40 and 60 m). The flux
375 of MnOx-like particles at 110 and 180 m was two orders of magnitude larger in the GB than in
376 the LD (Table 4). In the GB, MnOx-like particles were present in the sediment traps at 110 m and
377 180 m. They occurred as single particles and forming aggregates with each other and other
378 particles such as TEP (Figure 6a,e), phytoplankton cells, or detrital material. The ESD of MnOx-
379 like particles and aggregates ranged from 0.6 to 167 μm (median 2.8 μm) at 110 m and from 0.6
380 to 153 μm (median 3.3 μm) at 180 m. In the LD, only a few, single MnOx-like particles were
381 observed at 110, their size ranged from 0.6 to 16.5 mm (median 1.8) (Table 4).
382 Total hydrolyzable amino acids (TAA) flux ranged from 371±12 to 501± 33 μmol $m^{-2}d^{-1}$ in the
383 GB and from 502± 84 to 785± 54 μmol $m^{-2}d^{-1}$ in the LD (Fig. 7a). In the GB, the flux decreased
384 with depth whereas, in the LD, the TAA flux at 40 m was lower than at 60 m and decreased with
385 depth from 60 to 180 m (Fig. 7b). Vertical profile of TCHO flux was similar in both stations. The
386 TCHO flux varied between 303± 8 and 428± 14 μmol $m^{-2}d^{-1}$ in the GB (Fig. 7a) and between
387 503± 19 and 584± 8 μmol $m^{-2}d^{-1}$ in the LD (Fig. 7b). In both stations, TCHO flux increased from
388 40 to 110 m, where the highest TCHO flux was measured, and then TCHO flux decreased at 180
389 m. The TCHO flux at 180 m was 22% higher than at 40 m in the GB, and the same that at 40 m in
390 the LD.
391 3.5. *Chemical composition of sinking and suspended OM*

The molar ratios of suspended and sinking OM may be compared to the classical Redfield ratio for living plankton (106C: 16N: P; Redfield et al., 1963). Sinking OM was slightly above Redfield ratios at both stations. The POC:PN ratio of the sinking OM in both GB and LD were not significantly different. In the GB, the POC:PN ratio of the sinking OM increased with depth from 9.8 to 12.6. Contrastingly, in the suspended OM, POC:PN ratios were higher in the GB compared to the LD ($p<0.001$; Mann–Whitney U-test). In the GB, the POC:PN ratio of suspended OM varied between 8.4 and 12 without a clear trend with depth; while in the LD, decreased with depth from 8.7 (at 1m) to 6.2 (at 400m), and a slightly higher value of 7.8 was observed at 430 m. In the LD the POC:PN of sinking OM was significantly lower than in suspended OM ($p<0.001$). The POC:POP molar ratio of sinking OM was lower ($p<0.05$) in the GB than in the LD; and it was higher ($p<0.01$) in sinking than in suspended OM in the LD (Table 5). The POC:BSi molar ratio was lower in sinking than in suspended OM in both stations (GB: $p<0.05$; LD: $p<0.01$). In sinking OM, the POC:BSi ratio was below Redfield value, whereas in suspended OM it was above Redfield ratio (Table 5). The PN:POP molar ratio was lower in sinking OM than in suspended OM in both stations ($p<0.001$). In sinking OM this value was always below the Redfield ratio, while in suspended OM, it was always above the Redfield ratio.

At both stations, the fraction of sinking POC composed of AA was larger than in suspended OM. Similarly, the C contained in CHO made up a larger percentage in sinking OM than in suspended OM (Table 5). The amino acid-based degradation index (DI, Dauwe et al., 1999) in sinking OM varied from 0.1 to 1.14 and was higher than in suspended OM (-1.25 to -0.42). The DI was higher in the GB than in the LD in sinking and suspended OM. In the sinking OM of the GB, the DI decreased with depth but in the LD was more positive at 110m than at 60 m (Table 5).

4. Discussion

In this study, we described the results of 1) the characterization of the surface biogeochemical conditions and the sinking particles produced in the euphotic zone of the GB and the LD, during early summer 2015, 2) the flux, and vertical profile of sinking and suspended particles in the two basins. Our results suggested that the intrusion of oxygenated water to the GB associated with the

2014/2015 MBI caused changes in the water chemistry that affected the chemical composition and degradation stage of the sinking and suspended OM. This resulted in differences in the composition and magnitude of the sinking particle flux between GB and LD.

4.1 Characterization of biogeochemical conditions in GB and LD

Temperature, O_2, and inorganic nutrient concentrations were similar in euphotic zone (upper 20 m) at both stations. Moreover, though there were slight differences in biogeochemical conditions, such as phytoplankton biomass, phytoplankton composition and concentration and chemical composition of POM, in the surface water column, those were not significant. The concentration of Chl *a* (Fig. 3) and the abundance of picophytoplankton and nanophytoplankton (Table 2) were slightly higher (20 and 10 % respectively) in the GB than in the LD. This agrees with estimates of integrated total primary production, which were 10% larger in the GB (380 mg C m^{-2} d^{-1}) than in the LD (334 mg C m^{-2} d^{-1}; Piontek et al., unpublished). At both stations, picophytoplankton dominated the small phytoplankton (Table 2). These findings coincide with what was described previously for early summer in the Baltic Sea that indicate that during this period the productivity is sustained mostly by nano- and picophytoplankton communities (Leppänen et al., 1995) which co-existed with cyanobacteria and other phytoplankton species (Kreus et al. 2015). Microscopic analysis of larger phytoplankton (>5 μm), on the other hand, showed that filamentous cyanobacteria *Aphanizomenon* sp. (up to 200 μm large) was the dominant type on this size fraction in the upper 40 m (Table 3). *Aphanizomenon* sp. and *Nodularia spumigena*, are known to form summer blooms in the Baltic Sea, where they accumulate at the sea surface of the thermally stratified water column (Bianchi et al., 2000; Nausch et al., 2009; Wasmund, 1997). The medians of the cell abundance of total phytoplankton (>5 μm, table 3) in the upper 40 m of the water column were not significantly different (p=0.74) in the GB and the LD.

POC, PN, POP, BSi were slightly higher in the surface waters of the GB than in the LD; while TEP and CSP concentrations in the surface waters were similar at both stations (Fig. 3). The concentration of TEP was higher than of CSP, both types of gel-like particles were most abundant

445 in the euphotic zone indicating a phytoplankton origin. In the surface water column, TEP
446 concentrations (48 and 62 μg X.G. Eq. L^{-1} in the GB and the LD, respectively) were 69 and 76%
447 lower than the value previously reported for summer in the central Baltic Sea in June (200 μg
448 X.G. Eq. L^{-1}) (Engel et al., 2002). Likewise, our dissolved inorganic nitrogen concentrations were
449 below the detection limit in the surface; however phosphate concentrations were higher (0.2-0.65
450 μM) than the ones on the Engel et al. (2002) study. Mari and Burd (1998) reported that TEP
451 concentration peaked during the spring bloom and in summer in the Kattegat. TEP production
452 may be enhanced by enviromental conditions such as nutrient limitation (Mari et al., 2005;
453 Passow, 2002), which are characteristic of late summer in the Baltic Sea (Mari and Burd 1998).
454 Surface satellite-derived Chl-a concentrations in the Gotland Deep indicate that our samples were
455 collected during Chl-a peak in mid-June (8–10 μg L^{-3}). Chl-*a* concentrations increased constantly
456 from mid-May to the sampling period (Le Moigne et al., 2017), thus, likely TEP concentrations
457 had not reached the usually higher summer value yet since the high concentration of Chl-a and
458 presence of phosphate in the water column may suggest that the PP was not nutrient limited.
459 Another possible explanation for the rather low concentrations of TEP could be that TEP may be
460 removed from the surface by aggregation and subsequent sedimentation during the spring bloom
461 due to the high abundance of cells and detrital particles during this time (Engel et al., 2002).

462 Although the composition and amount of OM in the surface waters at the two trap stations were
463 similar, below the euphotic zone (40 m) the vertical profile of nutrients and POM concentrations
464 were clearly different; likely due to the 2014/2015 MBI (Holtermann et al., 2017) that reached the
465 deep waters of the GB. This inflow changed the salinity in the deepest waters and the vertical
466 distribution of O_2 increasing its concentrations below140 m and constraining the oxygen-deficient
467 layers from 74 m to 140 m depth. The water intrusion showed similar features as the new water
468 masses and water pushed out of the Bornholm Basin (Schmale et al., 2016). The combination of
469 physical effects (the displacement of water masses, turbulent mixing and lateral transport) and the
470 consequent development of redox conditions through 2015 may have impacted the distribution of

MnOx and POM in the GB. In contrast, the LD maintained permanent suboxic (<5 μmol L^{-1}) waters below 74 m and hydrogen sulfide was detectable at 180 and 250 m (Fig. 2).

MBIs can have a major impact on nutrient recycling. In the GB nitrate concentration increased possibly as a consequence of the oxidation of reduced nitrogen compounds (e.g., ammonium, ammonia and organic nitrogen compounds like urea) (Le Moigne et al., 2017) that accumulated during the stagnation (anoxic) period previous to the MBI (Hannig et al., 2007). Phosphorus could bind to iron hydroxides and MnOx and settle down during oxic conditions, building up a phosphate pool in the sediments that later on when the O_2 decreases close to the sediments, it may become a source of phosphate (Gustafsson and Stigebrandt, 2007). In addition to changes in O_2 concentration, the MBI altered the redox conditions in the GB creating a secondary redoxcline at 140 m, where the O_2 and the MnOx-like particles concentration increased (Fig. 4a). One consequence of those changes is the vertical extension of the layer in which MnOx aggregates could form. A previous study showed that MnOx might precipitate from the water column of the GB following a MBI event (Lenz et al., 2015). Scavenging of phosphate into Mn or Fe oxides had been shown in previous studies (Neretin et al., 2003). Moreover, Gustafsson and Stigebrandt, 2007 showed that there is a downward flux of phosphate, associated with particulate iron and MnOx, from the oxygenated water column to the anoxic deep waters. On the other hand, the intrusion of oxygenated water masses associated with the MBI caused turbulent mixing the deep water of the GB. Myllykangas et al. (2017) reported that following the 2014/2015 MBI, the GB experienced the displacement of stagnant water masses by the new water masses intruded during the MBI. Thus, the low concentrations of silicate and phosphate that we measured in the deep waters of the GB may also be a direct consequence of the intrusion of oxygenated, low-nutrient waters associated with the MBI. In contrast, in the LD, the water column remained suboxic down the sea floor (430 m), below the oxycline an increase of ammonium was observed (Fig.2b) which could be an indicator for anaerobic respiration of OM, e.g., denitrification (Bonaglia et al., 2016; Hietanen et al., 2012).

In summary, although the GB and the LD had similar surface conditions in terms of phytoplankton production and POM stocks, during this study, we found differences the vertical concentration of nutrients (Fig. 2) and POM (Fig. 3) in the GB, ventilated by the MBI, relative to the LD, a station that remains suboxic. Our results suggest that physical processes and differences in the vertical profile of O_2 may modify the redox conditions of the water column, enhance the formation of MnOx-like particles (Fig. 4) that may aggregate with POM in the GB (or transported to the GB by the inflow) influencing the vertical distribution of POM in the water column.

4.2 Potential influence of O_2 concentration and redox conditions on sinking fluxes of POM in the GB and the LD

During this study, we also investigated the effect of different O_2 concentrations and redox conditions on the fluxes of particles. Our measurement of carbon flux at 40 m, below the euphotic zone, were 11.7±0.82 mmol C m^{-2} d^{-1} in the GB and 19.8±1.22 mmol C m^{-2} d^{-1} in the LD. Extrapolating those measurements to annual flux we obtain 4.37±0.31 mol C m^{-2} a^{-1} in the GB and 7.44±0.46 mol C m^{-2} a^{-1} in the LD. Our results from the LD are in the same range that the long-term annual estimations from models that varied between 3.8 to 4.2 mol C m^{-2} d^{-1} (Kreus and Schartau, 2015; Sandberg et al., 2000; Stigebrandt, 1991) for the Baltic Sea; however, the estimations based on our results from the GB are higher than the C fluxes predicted by those models.

The vertical flux of POM was different in the two studied stations. In the GB, the POM fluxes showed distinct trends with depth; while the POC flux slightly decreased from below the upper oxycline (60 m) to 180 m, the PN flux slightly increased with depth. On the other hand, the fluxes of POP, BSi, Chl *a* and TEP showed a distinctive peak in the core of the OMZ (at 110 m). In the LD, the POC flux decreased in the fully oxygenated upper water column (between 40 and 55 m), and remained relatively constant in the OMZ (between 60 and 180 m); PN flux, steadily decreased with depth. Similar to GB, but smaller, a peak of POP, BSi, Chl *a* and TEP fluxes was observed at 110 m. This high flux of POM at 110 m in both stations coincided with the

appearance of dark, star-shaped particles, particularly evident at GB (Fig. 6a, e), but also present in LD, which may correspond to MnOx particles enriched in OM that have been described in the GB and the LD before (Neretin et al., 2003; Pohl et al., 2004). Similar to the vertical distribution on POM in the water column discussed in the section above, differences in POM fluxes between stations are likely associated with the large inflow of oxygen-rich saltwater that displaced the old, stagnant water masses and changed the chemistry of the water column (Myllykangas et al., 2017). Under euxinic (*e.i.*, no MBI) conditions, the maximum concentration of particulate Mn is found at the depth of the oxycline (Glockzin et al., 2014). Below the oxycline, and due to the hydrogen sulfide (H_2O) presence, the particulate Mn concentration decreased drastically. During this study, we observed high concentration of MnOx particles flux at 110 and 180 m (Table 5) in the GB; this result agreed with the high flux of particulate Mn measured in sediment traps located at 186 m in June 2015 (Dellwig et al., 2018). The oxygenation of the deep water layers of the GB by the MBI caused the absence of H_2S (Schmale et al., 2016) and provided the redox conditions to measured high MnOx flux in the sediment trap located in the core of the OMZ (110 m) and at 180 m. There were two possible sources of MnOx in the GB associated with the 2014/2015 MBI, on one hand, the lateral transport of low-density aggregates formed by MnOx and OM (Glockzin et al., 2014), and on the other hand, the remarkable *in-situ* formation and deposition of MnOx from dissolved Mn, which inventory drastically decreased in the water column due to the change in redox conditions (Dellwig et al., 2018). In clear contrast to the oxygenated deep layers of the GB, in the LD, we measured H_2S at 180 m, this could explain why although those aggregates were present in this station below the oxycline (*i.e.,* 70 m) at 110 m, they dissolved in sulfidic waters, thus were not as abundant, and did not form aggregates with TEP (Fig.6c).

The presence of MnOx-containing aggregates enriched in OM (see TEP fluxes, Fig 6c) may have implications for the vertical flux of C and N in a stratified system with a pelagic redoxcline like the Baltic Sea. Under steady state, the upward diffusion and oxidation rate of the dissolved Mn are balanced by the sinking and dissolution rate of MnOx. During the Mn-oxidation, the POM could aggregate with the MnOx including particulate elements, and trace metals. Then, in the

sulfidic waters, slow-sinking MnOx enriched in OM will be dissolved liberating the OM and altering the vertical distribution and the flux of all associated particle elements (Glockzin et al., 2014). For example, in the Cariaco Basin, total particulate phosphorus reached their maximum flux in sediment traps close to the redoxcline (Benitez-Nelson et al., 2004; Benitez-Nelson et al., 2007). MnOx formation and scavenging of trace metal may be a relevant mechanism for transfer trace metals from the oxygenated to the anoxic deep waters (Dellwig et al., 2010). Moreover, even in the anoxic zone, the abundant aggregate associated bacteria (Grossart et al., 2006) could partially or completely degrade the organic compounds in those particles using NO_3^- or MnOx as an electron acceptor. This may explain why we observed a clear peak in the flux of POP, BSi, Chl a (Fig. 3a, b), TEP (Fig. 6a) and TCHO (Fig. 7a) at 110 m followed by a small decrease at 180 m in the GB. In the LD a smaller increment in the flux of POP, BSi (Fig. 3d), TEP (Fig. 6c) and TCHO (Fig. 7b) was also observed. The vertical fluxes of those compounds coincided with the abundance of MnOx particles; we assume that the MnOx aggregated not only with TEP as described before (Glockzin et al. 2014) and observed in this study (Fig. 6a) but also with POP, BSi, Chl *a*, and TCHO. On the other hand, nitrogen-rich components of POM like PN (Fig. 3a), TAA (Fig. 7a), and CSP (Fig. 6a) gradually decreased with depth in the GB, suggesting that those compounds were less scavenge by MnOx-OM rich aggregates.

Primary production (PP) in the GB was 10% higher than in LD during our study (Piontek et al. unpublished data). However, the POC flux below the euphotic zone (at 40 m) was 42% higher in LD than in GB and comparable at both stations at 180 m. The fraction of PP exported as POC is termed export production (*e-ratio*) (Buesseler et al., 1992), and it is calculated as the POC flux below the euphotic zone divided by the primary production. The *e-ratio* was calculated here using the ^{14}C based PP (Piontek et al. unpublished data) and carbon flux at 40 m (shallowest sediment trap depth, considered at the base of the euphotic zone). The *e-ratio* was 0.41 in the GB and 0.77 in the LD*; i.e.*, in GB 41% of the primary production was exported as POC below the euphotic zone (40 m) versus 77% in the LD. This suggests that a higher proportion of the primary production was remineralized in the euphotic zone of the GB compared with the LD. On the other

577 hand, the transfer efficiency of POC to the deeper water column (*i.e.* the ratio of POC flux at180
578 m over POC flux at 40 m) was higher in the GB (115%) than in the LD (69%). The transfer
579 efficiency of POM is largely controlled by the remineralization rate and the sinking velocity of
580 particles (De La Rocha and Passow, 2007; McDonnell et al., 2015; Trull et al., 2008). The higher
581 POC transfer efficiency in the GB than in the LD can be attributable to differences in the sinking
582 velocities of the particles in those two stations. Particulate MnOx may sink through the redoxcline
583 in the GB (Neretin et al., 2003) acting as ballast material and nucleus for MnOx-OM rich
584 aggregates formation. Those aggregates could have sunk more quickly, limiting the time spent in
585 the water column and the degradation by particle- attached microbes. Assuming that MnOx had a
586 density between 1.5 and 2.0 g cm^{-3} (Glockzin et al., 2014). The largest particles measured in GB
587 (167 μm, Table 4) will have a sinking velocity based in Stokes' law between 508 and 1014 m d^{-1}.
588 If we considered a mixed aggregate that is 50% TEP, density 0.9 g cm^{-3} (Azetsu-Scott and
589 Passow, 2004) and 50% MnOx (density 1.5 g cm^{-3}), its density would be 1.2 g cm^{-3}, and its
590 theoretical sinking velocity will be 204 m d^{-1}. This indicates that theoretically, the largest mix
591 aggregates composed of MnOx and TEP observed in the GB could reach 180 m (the location of
592 our deepest sediment trap) in less than one day. However, the average measured sinking velocity
593 of MnOx in the laboratory for particles between 2 and 20 μm was 0.76 m d^{-1}, this is significantly
594 lower than the theoretical value (Glockzin et al., 2014). Glockzin et al. (2014) suggested that the
595 star shape and the content of OM were responsible for the lower than predicted sinking velocity.
596 There is no information about the amount of OM relatively to MnOx particles in those mix
597 aggregates, or how the MnOx to OM ratio may affect the density and sinking velocity of larger
598 aggregates like the ones we observed. Due to the shape and size of MnOx-OM aggregates
599 observed in our study (Fig. 6e), we could assume those are the same type of aggregates described
600 before by Glockzin et al. (2014). Although we did not measure the sinking velocity of those
601 aggregates, we did observe a higher abundance of them associated with TEP at 110 and 180 m in
602 the GB than in the LD. The formation of these organic matter rich MnOx aggregates could
603 represent an additional mechanism (see introduction) to explain why the efficiency of the OM

export is different under anoxic that under oxic conditions in the Baltic Sea. The oxygenation of anoxic deep water in the GB caused by the 2014/2015 MBI, may have led to an enhanced precipitation of manganese, iron and phosphorus particles (Dellwig et al., 2010; Dellwig et al., 2018). For example, the formation of P-rich, metal oxides precipitates occur in the anoxic waters of the Black Sea (Shaffer, 1986) and Cariaco Basin (Benitez-Nelson et al., 2004; Benitez-Nelson et al., 2007) were higher concentration of particulate inorganic and organic phosphorus have been observed in sediment traps close to the redoxcline.

4.3 Differences on composition and lability of sinking and suspended organic matter in the GB and the LD

In the sections above, we discussed how similar were biogeochemical conditions and the size of the surface POM pool in both the GB and the LD. We then looked at how the sinking flux of OM was affected by the different O_2 concentrations in the water column. We now focus on the influence of O_2 in the chemical composition of sinking and suspended POM. Suspended or slow sinking POM, that spend more time in the water column, should theoretically, show a larger degree of degradation (Goutx et al., 2007). Relative to the Redfield molar ratio: 106 POC:16 PN:POP, OM showed an enrichment in carbon, especially in sinking particles from the LD and suspended OM from the GB (Table 5). Our measured values of POC:PN (~10) and POC:POP (between 89 and 506) in suspended OM coincide with the simulated ratio reported by Kreus et al. (2015) immediately after the culmination of the spring bloom, those relatively high ratios are consequence of the nitrogen depletion and are characteristic during the summer in the Baltic Sea. The same study had suggested that POC:POP higher than Redfield ratio might lead to an enhancement of particle export (Kreus et al., 2015), however, no direct observations had confirmed this hypothesis. Our measurements showed that the relative higher POC:POP ratios in sinking OM from LD, compared with the GB, do not lead to a higher transfer efficiency at this station. Compared to the suspended OM in the LD, the POP content was lower in the GB, possible related to scavenging of POP into MnOx aggregates (see section 3.4).

The TAA based degradation index, DI (Dauwe et al. 1999) covers a wide range of alteration stages; the more negative the DI, the more degraded the samples, positive DI indicates fresh organic matter. In our study, the sediment trap material had a DI between 0.10 and 1.14, while suspended OM has a DI between -0.26 and -1.25 (Table 4). These values coincide with what reported earlier by Dauwe et al. (1999), and indicate that: first, the sinking particles collected in the sediment traps were less altered (they have a more positive DI) than the suspended OM collected in the Niskin bottle. Second, sinking particles from the GB were fresher than the ones from the LD, and the degradation stage increased with depth in both stations. The higher contribution of AA and CHO to the POC pool in sinking than in suspended OM and the AA- DI indicates that suspended OM was more degraded than sinking OM. The highest degree of degradation in suspended OM and sinking OM from the LD may be the result of a long time that light suspended OM or slow sinking particles spend exposed to degradation in fully oxygenated surface waters than dense, fast sinking particles collected in sediment traps.

The higher abundance of aggregates, formed by a combination of MnOx-like particles and OM, observed at 110 and 180 m in the GB could act as bacteria hot spots that combined with a higher O_2 concentration in the GB may increase the microbial degradation on sinking particles collected in the GB. However, the AA-DI, indicated that sinking OM was less altered and therefore more labile than the sinking OM in the LD. This implied that in addition to the higher transfer efficiency of POC in the GB (see discussion above); the OM reaching the seafloor was fresher and less degraded. This supports the idea that mix aggregates composed by MnOx and OM may be larger and faster sinking than the previously described by Glockzin et al. (2014). This explanation is mostly speculative, and based on the observation of large mixed aggregates in the 110 and 180 m traps (Fig. 6, Table 4). However, as mention in the previous section, further work on directly determines sinking velocity is required to prove this hypothesis.

Conclusion

Fluxes and composition of sinking particles were different in two deep basins in the Baltic Sea: the GB and the LD during early summer 2015. The two stations had similar surface characteristics and POM stock; however, at depth, the vertical profile of the O_2 concentration was different. The 2014/2015 MBI supplied oxygen-rich waters to the GB transporting solid material from the and modifying the O_2 vertical profile and the redox conditions in the otherwise permanent suboxic deep waters. This event did not affect the LD allowing the comparing POM fluxes and composition under two different O_2 concentrations with similar surface water conditions. Export efficiency (*e-ratio*) derived from *in-situ* PP measurements and POC flux derivate from sediment traps indicated higher export efficiency in LD than in GB. However, the transfer efficiency (POC flux at 180 m over POC flux at 40 m) suggested that under anoxic conditions found in the LD, a smaller portion of the POC exported below the euphotic zone was transferred to 180 m than under re-oxygenated conditions present in the GB. The 2014/2015 MBI also transport solid Mn from shallower areas towards the GB deep that may have contributed to the higher abundance of MnOx-OM in the GB. Our results suggest that a new possible mechanism to explain the differences in the OM fluxes under different O_2 concentration could be the formation and prevalence of aggregates composed of MnOx and organic matter in the GB. Those aggregates were significantly larger and more abundant in the GB compared to the LD where sulfidic waters constrained their presence. We propose that after a MBI in the GB, the aggregates containing MnOx-like particles and organic matter could have reached the sediments relatively fast and unaltered, scavenging not only phosphorus and TEP, as described previously, but also other organic compounds. The remineralization of this organic matter reaching the sediments may contribute to the quick re-establishment of anoxic conditions in the sediment-water interface in the GB. The relevance of this process needs to be further investigated in order to be included in O_2 budget and long-term predictions of the MBI impact in the O_2 and OM cycles.

Author Contributions

C.C.N. performed deployments, analyzed samples and wrote the manuscript. F.A.C.L.M, performed deployments and contributed to the writing of the manuscript. A.E designed and conducted the scientific program at sea and discussed and commented on the manuscript.

Acknowledgements

This research was supported by the DFG Collaborative Research Center 754 "Climate-Biogeochemistry Interactions in the Tropical Ocean" (to A.E., C.C.N. and F.A.C.L.M), by a Fellowship of the Excellence Cluster 'The Future Ocean' (CP1403 to F.A.C.L.M.), and by a DAAD short term grant (57130097 to C.C.N.). We thank Jon Roa, Tania Klüver, Scarlett Sett, Angela Stippkugel, Carola Wagner, Clarissa Karthäuser, Moritz Ehrlich, Sonja Endres, Hannes Wagner, Ruth Flerus, Sven Sturm and Christian Begler for support during traps preparation and deployments, help with experiment or analyzed samples. We Thank Judith Piontek for her contribution to the design of the scientific program at sea, Jaime Soto- Neira for useful discussion and help with figure preparation and Cindy Lee for helpful advices.

References

Alldredge, A. L., Passow, U., and Logan, B. E.: The abundance and significance of a class of large, transparent organic particles in the ocean, Deep Sea Research Part I: Oceanographic Research Papers, 40, 1131-1140, 1993.

Andersen, J. H., Carstensen, J., Conley, D. J., Dromph, K., Fleming-Lehtinen, V., Gustafsson, B. G., Josefson, A. B., Norkko, A., Villnäs, A., and Murray, C.: Long-term temporal and spatial trends in eutrophication status of the Baltic Sea, Biological Reviews, 92, 135-149, 2017.

Armstrong, R. A., Lee, C., Hedges, J. I., Honjo, S., and Wakeham, S. G.: A new, mechanistic model for organic carbon fluxes in the ocean based on the quantitative association of POC with ballast minerals, Deep Sea Research Part II: Topical Studies in Oceanography, 49, 219-236, 2002.

Azetsu-Scott, K. and Passow, U.: Ascending marine particles: Significance of transparent exopolymer particles (TEP) in the upper ocean, Limnology and Oceanography, 49, 741-748, 2004.

Benitez-Nelson, C. R., O'Neill, L., Kolowith, L. C., Pellechia, P., and Thunel, l. R.: Phosphonates and particulate organic phosphorus cycling in an anoxic marine basin, Limnology and Oceanography, 49, 1593-1604, 2004.

Benitez-Nelson, C. R., O'Neill Madden, L. P., Styles, R. M., Thunell, R. C., and Astor, Y.: Inorganic and organic sinking particulate phosphorus fluxes across the oxic/anoxic water column of Cariaco Basin, Venezuela, Marine Chemistry, 105, 90-100, 2007.

Bianchi, T. S., Engelhaupt, E., Westman, P., Andrén, T., Rolff, C., and Elmgren, R.: Cyanobacterial blooms in the Baltic Sea: Natural or human-induced?, Limnology and Oceanography, 45, 716-726, 2000.

Bonaglia, S., Klawonn, I., Brabandere, L. D., Deutsch, B., Thamdrup, B., and Brüchert, V.: Denitrification and DNRA at the Baltic Sea oxic–anoxic interface: Substrate spectrum and kinetics, Limnology and Oceanography, 61, 1900-1915, 2016.

Boyd, P. W. and Trull, T. W.: Understanding the export of biogenic particles in oceanic waters: Is there consensus?, Progress in Oceanography, 72, 276-312, 2007.

Brettar, I. and Rheinheimer, G.: Denitrification in the Central Baltic: evidence for H ₂ S-oxidation as motor of denitrification at the oxic-anoxic interface, Marine Ecology Progress Series, 77, 157-169, 1991.

Buesseler, K. O., Bacon, M. P., Kirk Cochran, J., and Livingston, H. D.: Carbon and nitrogen export during the JGOFS North Atlantic Bloom experiment estimated from 234Th: 238U disequilibria, Deep Sea Research Part A. Oceanographic Research Papers, 39, 1115-1137, 1992.

Carstensen, J., Andersen, J. H., Gustafsson, B. G., and Conley, D. J.: Deoxygenation of the Baltic Sea during the last century, Proceedings of the National Academy of Sciences, 111, 5628-5633, 2014a.

Carstensen, J., Conley, D. J., Bonsdorff, E., Gustafsson, B. G., Hietanen, S., Janas, U., Jilbert, T., Maximov, A., Norkko, A., Norkko, J., Reed, D. C., Slomp, C. P., Timmermann, K., and Voss, M.: Hypoxia in the Baltic Sea: Biogeochemical Cycles, Benthic Fauna, and Management, AMBIO, 43, 26-36, 2014b.

Cavan, E. L., Trimmer, M., Shelley, F., and Sanders, R.: Remineralization of particulate organic carbon in an ocean oxygen minimum zone, Nature Communications, 8, 14847, 2017.

Cisternas-Novoa, C., Lee, C., and Engel, A.: A semi-quantitative spectrophotometric, dye-binding assay for determination of Coomassie Blue stainable particles, Limnology and Oceanography: Methods, 12, 604-616, 2014.

Conley, D. J., Björck, S., Bonsdorff, E., Carstensen, J., Destouni, G., Gustafsson, B. G., Hietanen, S., Kortekaas, M., Kuosa, H., Markus Meier, H. E., Müller-Karulis, B., Nordberg, K., Norkko, A., Nürnberg, G., Pitkänen, H., Rabalais, N. N., Rosenberg, R., Savchuk, O. P., Slomp, C. P., Voss, M., Wulff, F., and Zillén, L.: Hypoxia-Related Processes in the Baltic Sea, Environmental Science & Technology, 43, 3412-3420, 2009.

Dauwe, B., Middelburg, J. J., Herman, P. M. J., and Heip, C. H. R.: Linking diagenetic alteration of amino acids and bulk organic matter reactivity, Limnology and Oceanography, 44, 1809-1814, 1999.

De La Rocha, C. L. and Passow, U.: Factors influencing the sinking of POC and the efficiency of the biological carbon pump, Deep Sea Research Part II: Topical Studies in Oceanography, 54, 639-658, 2007.
Dellwig, O., Leipe, T., März, C., Glockzin, M., Pollehne, F., Schnetger, B., Yakushev, E. V., Böttcher, M. E., and Brumsack, H.-J.: A new particulate Mn–Fe–P-shuttle at the redoxcline of anoxic basins, Geochimica et Cosmochimica Acta, 74, 7100-7115, 2010.
Dellwig, O., Schnetger, B., Meyer, D., Pollehne, F., Häusler, K., and Arz, H. W.: Impact of the Major Baltic Inflow in 2014 on Manganese Cycling in the Gotland Deep (Baltic Sea), Frontiers in Marine Science, 5, 2018.
Devol, A. H. and Hartnett, H. E.: Role of the oxygen-deficient zone in transfer of organic carbon to the deep ocean, Limnology and Oceanography, 46, 1684-1690, 2001.
Dittmar, T., Cherrier, J., and Ludwichowski, K. U.: The analysis of amino acids in seawater. In: Practical guidelines for the analysis of seawater Wurl, O. and Raton, B. (Eds.), CRC Press, 2009.
Dollhopf, M. E., Nealson, K. H., Simon, D. M., and Luther, G. W.: Kinetics of Fe(III) and Mn(IV) reduction by the Black Sea strain of Shewanella putrefaciens using in situ solid state voltammetric Au/Hg electrodes, Marine Chemistry, 70, 171-180, 2000.
Dugdale, R. C. and Goering, J. J.: Uptake Of New And Regenerated Forms Of Nitrogen In Primary Productivity, Limnology and Oceanography, 12, 196-206, 1967.
Emeis, K. C., Struck, U., Leipe, T., Pollehne, F., Kunzendorf, H., and Christiansen, C.: Changes in the C, N, P burial rates in some Baltic Sea sediments over the last 150 years—relevance to P regeneration rates and the phosphorus cycle, Marine Geology, 167, 43-59, 2000.
Engel, A.: The role of transparent exopolymer particles (TEP) in the increase in apparent particle stickiness (α) during the decline of a diatom bloom, Journal of Plankton Research, 22, 485-497, 2000.
Engel, A., Meyerhöfer, M., and von Bröckel, K.: Chemical and Biological Composition of Suspended Particles and Aggregates in the Baltic Sea in Summer (1999), Estuarine, Coastal and Shelf Science, 55, 729-741, 2002.
Engel, A. and Schartau, M.: Influence of transparent exopolymer particles (TEP) on sinking velocity of Nitzschia closterium aggregates, Marine Ecology Progress Series, 182, 69-76, 1999.
Engel, A., Wagner, H., Le Moigne, F. A. C., and Wilson, S. T.: Particle export fluxes to the oxygen minimum zone of the eastern tropical North Atlantic, Biogeosciences, 14, 1825-1838, 2017.
Eppley, R. W. and Peterson, B. J.: Particulate organic matter flux and planktonic new production in the deep ocean, Nature, 282, 677, 1979.
Glockzin, M., Pollehne, F., and Dellwig, O.: Stationary sinking velocity of authigenic manganese oxides at pelagic redoxclines, Marine Chemistry, 160, 67-74, 2014.
Goutx, M., Wakeham, S. G., Lee, C., Duflo, s. M., Guigue, C., Liu, Z., Moriceau, B., Sempére, R., Tedetti, M., and Xue, J.: Composition and degradation of marine particles with different settling velocities in the northwestern Mediterranean Sea, Limnology and Oceanography, 52, 1645-1664, 2007.
Grossart, H. P., KiÃƒÂ¸rboe, T., Tang, K. W., Allgaier, M., Yam, E. M., and Ploug, H.: Interactions between marine snow and heterotrophic bacteria: aggregate formation and microbial dynamics, Aquatic Microbial Ecology, 42, 19-26, 2006.
Günter, J., Zubkov, M. V., Yakushev, E., Labrenz, M., and JÜrgens, K.: High abundance and dark CO2 fixation of chemolithoautotrophic prokaryotes in anoxic waters of the Baltic Sea, Limnology and Oceanography, 53, 14-22, 2008.
Gustafsson, B. G. and Stigebrandt, A.: Dynamics of nutrients and oxygen/hydrogen sulfide in the Baltic Sea deep water, Journal of Geophysical Research: Biogeosciences, 112, 2007.
Hannig, M., Lavik, G., Kuypers, M. M. M., Woebken, D., Martens-Habbena, W., and JÜrgens, K.: Shift from denitrification to anammox after inflow events in the central Baltic Sea, Limnology and Oceanography, 52, 1336-1345, 2007.
Hansen, H. P. and Koroleff, F.: Determination of nutrients. In: Methods of Seawater Analysis., Grasshoff, K., Kremling, K., and Ehrhardt, M. (Eds.), Willey-VCH, Weinheim, Germany, 1999.

Hansen, H. P. and Koroleff, F.: Determination of nutrients. In: Methods of Seawater Analysis, Wiley-VCH Verlag GmbH, 2007.
Hietanen, S., Jäntti, H., Buizert, C., Jürgens, K., Labrenz, M., Voss, M., and Kuparinen, J.: Hypoxia and nitrogen processing in the Baltic Sea water column, Limnology and Oceanography, 57, 325-337, 2012.
Holtermann, P. L., Prien, R., Naumann, M., Mohrholz, V., and Umlauf, L.: Deepwater dynamics and mixing processes during a major inflow event in the central Baltic Sea, Journal of Geophysical Research: Oceans, 122, 6648-6667, 2017.
Keil, R. G., Neibauer, J. A., Biladeau, C., van der Elst, K., and Devol, A. H.: A multiproxy approach to understanding the "enhanced" flux of organic matter through the oxygen-deficient waters of the Arabian Sea, Biogeosciences, 13, 2077-2092, 2016.
Knauer, G. A., Martin, J. H., and Bruland, K. W.: Fluxes of particulate carbon, nitrogen, and phosphorus in the upper water column of the northeast Pacific, Deep Sea Research Part A. Oceanographic Research Papers, 26, 97-108, 1979.
Kreus, M. and Schartau, M.: Variations in the elemental ratio of organic matter in the central Baltic Sea: Part II – Sensitivities of annual mass flux estimates to model parameter variations, Continental Shelf Research, 100, 46-63, 2015.
Kreus, M., Schartau, M., Engel, A., Nausch, M., and Voss, M.: Variations in the elemental ratio of organic matter in the central Baltic Sea: Part I—Linking primary production to remineralization, Continental Shelf Research, 100, 25-45, 2015.
Kullenberg, G. and Jacobsen, T. S.: The Baltic Sea: an outline of its physical oceanography, Marine Pollution Bulletin, 12, 183-186, 1981.
Le Moigne, F. A. C., Cisternas-Novoa, C., Piontek, J., Maßmig, M., and Engel, A.: On the effect of low oxygen concentrations on bacterial degradation of sinking particles, Scientific Reports, 7, 16722, 2017.
Legendre, L. and Gosselin, M.: New production and export of organic matter to the deep ocean: Consequences of some recent discoveries, Limnology and Oceanography, 34, 1374-1380, 1989.
Leipe, T., Tauber, F., Vallius, H., Virtasalo, J., Uścinowicz, S., Kowalski, N., Hille, S., Lindgren, S., and Myllyvirta, T.: Particulate organic carbon (POC) in surface sediments of the Baltic Sea, Geo-Marine Letters, 31, 175-188, 2011.
Lenz, C., Jilbert, T., Conley, D. J., Wolthers, M., and Slomp, C. P.: Are recent changes in sediment manganese sequestration in the euxinic basins of the Baltic Sea linked to the expansion of hypoxia?, Biogeosciences, 12, 4875-4894, 2015.
Lindroth, P. and Mopper, K.: High performance liquid chromatographic determination of subpicomole amounts of amino acids by precolumn fluorescence derivatization with o-phthaldialdehyde, Analytical Chemistry, 51, 1667-1674, 1979.
Logan, B. E., Passow, U., Alldredge, A. L., Grossartt, H.-P., and Simont, M.: Rapid formation and sedimentation of large aggregates is predictable from coagulation rates (half-lives) of transparent exopolymer particles (TEP), Deep Sea Research Part II: Topical Studies in Oceanography, 42, 203-214, 1995.
Long, R. A. and Azam, F.: Abundant protein-containing particles in the sea, Aquatic Microbial Ecology, 10, 213-221, 1996.
Mari, X. and Burd, A.: Seasonal size spectra of transparent exopolymeric particles (TEP) in a coastal sea and comparison with those predicted using coagulation theory, Marine Ecology Progress Series, 163, 13, 1998.
Mari, X., Passow, U., Migon, C., Burd, A. B., and Legendre, L.: Transparent exopolymer particles: Effects on carbon cycling in the ocean, Progress in Oceanography, 151, 13-37, 2017.
Mari, X., Rassoulzadegan, F., Brussaard, C. P. D., and Wassmann, P.: Dynamics of transparent exopolymeric particles (TEP) production by Phaeocystis globosa under N- or P-limitation: a controlling factor of the retention/export balance, Harmful Algae, 4, 895-914, 2005.

McDonnell, A. M. P., Boyd, P. W., and Buesseler, K. O.: Effects of sinking velocities and microbial respiration rates on the attenuation of particulate carbon fluxes through the mesopelagic zone, Global Biogeochemical Cycles, 29, 175-193, 2015.
Myllykangas, J. P., Jilbert, T., Jakobs, G., Rehder, G., Werner, J., and Hietanen, S.: Effects of the 2014 major Baltic inflow on methane and nitrous oxide dynamics in the water column of the central Baltic Sea, Earth Syst. Dynam., 8, 817-826, 2017.
Nausch, M., Nausch, G., Lass, H. U., Mohrholz, V., Nagel, K., Siegel, H., and Wasmund, N.: Phosphorus input by upwelling in the eastern Gotland Basin (Baltic Sea) in summer and its effects on filamentous cyanobacteria, Estuarine, Coastal and Shelf Science, 83, 434-442, 2009.
Neretin, L. N., Pohl, C., Jost, G., Leipe, T., and Pollehne, F.: Manganese cycling in the Gotland Deep, Baltic Sea, Marine Chemistry, 82, 125-143, 2003.
Passow, U.: Production of transparent exopolymer particles (TEP) by phyto- and bacterioplankton, Marine Ecology Progress Series, 236, 12, 2002.
Passow, U. and Alldredge, A. L.: A dye-binding assay for the spectrophotometric measurement of transparent exopolymer particles (TEP), Limnology and Oceanography, 40, 1326-1335, 1995.
Pohl, C., Löffler, A., and Hennings, U.: A sediment trap flux study for trace metals under seasonal aspects in the stratified Baltic Sea (Gotland Basin; 57°19.20'N; 20°03.00'E), Marine Chemistry, 84, 143-160, 2004.
Richardson, L. L., Aguilar, C., and Nealson, K. H.: Manganese oxidation in pH and O2 microenvironments produced by phytoplankton1,2, Limnology and Oceanography, 33, 352-363, 1988.
Sandberg, J., Elmgren, R., and Wulff, F.: Carbon flows in Baltic Sea food webs — a re-evaluation using a mass balance approach, Journal of Marine Systems, 25, 249-260, 2000.
Schmale, O., Krause, S., Holtermann, P., Power Guerra, N. C., and Umlauf, L.: Dense bottom gravity currents and their impact on pelagic methanotrophy at oxic/anoxic transition zones, Geophysical Research Letters, 43, 5225-5232, 2016.
Shaffer, G.: Phosphate pumps and shuttles in the Black Sea, Nature, 321, 515, 1986.
Stigebrandt, A.: Computations of oxygen fluxes through the sea surface and the net production of organic matter with application to the Baltic and adjacent seas, Limnology and Oceanography, 36, 444-454, 1991.
Strickland, J. D. and Parsons, T. R.: Determination of dissolved oxygen. In: A Practical Handbook of Seawater Analysis, Fisheries Research Board of Canada, 1968.
Strickland, J. D. H., Parsons, T. R., and Strickland, J. D. H.: A practical handbook of seawater analysis, Fisheries Research Board of Canada, Ottawa, 1972.
Thomas, H. and Schneider, B.: The seasonal cycle of carbon dioxide in Baltic Sea surface waters, Journal of Marine Systems, 22, 53-67, 1999.
Trull, T. W., Bray, S. G., Buesseler, K. O., Lamborg, C. H., Manganini, S., Moy, C., and Valdes, J.: In situ measurement of mesopelagic particle sinking rates and the control of carbon transfer to the ocean interior during the Vertical Flux in the Global Ocean (VERTIGO) voyages in the North Pacific, Deep Sea Research Part II: Topical Studies in Oceanography, 55, 1684-1695, 2008.
Turner, J. T.: Zooplankton fecal pellets, marine snow, phytodetritus and the ocean's biological pump, Progress in Oceanography, 130, 205-248, 2015.
van Mooy, B. A. S., Keil, R. G., and Devol, A. H.: Impact of suboxia on sinking particulate organic carbon: Enhanced carbon flux and preferential degradation of amino acids via denitrification, Geochimica et Cosmochimica Acta, 66, 457-465, 2002.
Wasmund, N.: Occurrence of cyanobacterial blooms in the baltic sea in relation to environmental conditions, Internationale Revue der gesamten Hydrobiologie und Hydrographie, 82, 169-184, 1997.
Wasmund, N. and Uhlig, S.: Phytoplankton trends in the Baltic Sea, ICES Journal of Marine Science, 60, 2003.
Wilhelm, W. L.: Die Bestimmung des im Wasser gelösten Sauerstoffes, Berichte der deutschen chemischen Gesellschaft, 21, 2843-2854, 1888.

Figure Captions

Figure 1. Monthly averaged Chl *a* distribution derived from VIIRS for June 2015 in the Baltic Sea. Black circle and "x" indicate the position of the trap deployment and the seawater collection respectively in Gotland Deep (GB) and Landsort Deep (LD). The lower panel shows the trajectory of the trap deployed at GB and LD.

Figure 2. Water column profiles at the location of the sediment trap deployments in (A) the GB, and (B) the LD. Left panel: oxygen (blue), temperature (red), and salinity (black). Middle panel: nitrate (NO_3), nitrite (NO_2), and ammonium (NH_4). Right panel: phosphate (PO_4), and silicate ($Si(OH)_4$). Grey lines indicate the depths at which we deployed sediment traps.

Figure 3. Particulate organic matter profiles in the water column at the location of the sediment traps deployments in the GB (A, B and C) and the LD (D, E and F). (A and D) particulate organic carbon (POC), particulate nitrogen (PN), and particulate organic phosphorus (POP). (B and E) chlorophyll a (Chl a) and biogenic silicate (BSi). (C and F) transparent exopolymeric particles (TEP) and Coomassie stainable particles (CSP). Grey lines as figure 2.

Figure 4. MnOx-like containing particles and O_2 concentration profiles in the water column at the location of the sediment traps deployments. (A) the GB and (B) the LD. Grey lines as in figure 3.

Figure 5. Particulate organic matter fluxes in the GB (A and B) and the LD (C and D) . (A and C) POC, PN and O_2. (B and D) POP, Chl a, and BSi.

Figure 6. TEP and CSP fluxes in the GB (A and B) and the LD (C and D). In addition to the vertical distribution of the flux, each profile is complemented with images captured under the microscope (200x) at each depth. Star-shaped MnOx-like particles are clearly visible in the GB associated to TEP (A), but not with CSP (B). MnOx-like particles were significantly less abundant in the LD (C and D). (F) A larger magnification (400x) image of MnOx-like particles at 110 m showing more detail on the shape of those particles and aggregates formed with TEP.

Figure 7. Total hydrolyzable amino acids (TAA) and total carohydrates (TCHO) fluxes in (A) the GB, and (B) the LD.

Table 1. Sediment traps deployment and recovery locations, dates, collection times and depths.

Station	Lat	Lon	Date	Station depth	Deployment time (d)	Trap depths (m)
Gotland Basin (GB)	57.21 °N	20.03 °E	08/06/2015	248 m	2	40A, 40B, 60, 110, and 180m
	57.27 °N	20.25 °E	10/06/2015			
Landsort Deep (LD)	58.69 °N	18.55 °E	15/06/2015	460 m	1	40A, 40B, 55, 110, and 180m
	58.68 °N	18.68 °E	16/06/2015			

Table 2. Abundance of chlorophyll and phycoerythrin containing pico- and nanoplankton measured by flow-cytometry in the GB and the LD.

	Depth (m)	Phytoplankton (cells mL^{-1})			Cyanobacteria-like (cells mL^{-1})		
		picoplankton	nanoplankton	Total	picoplankton	nanoplankton	Total
GB	1	87963	2097	90060	5225	731	5956
	10	94369	2628	96997	8795	920	9716
	40	4999	68	5067	2174	69	2243
	60	4125	35	4160	1990	42	2032
	80	599	7	606	238	15	253
	110	594	7	601	326	29	356
	140	1144	14	1158	356	2	358
	180	908	9	917	366	20	385
	220	2270	19	2289	1063	34	1097
LD	1	92359	2283	94642	834	177	1011
	10	86426	1708	88134	2990	232	3223
	40	2022	92	2114	2243	69	2312
	60	1524	62	1586	1294	24	1318
	70	908	43	951	613	17	630
	110	1735	82	1817	1181	17	1198
	180	1339	75	1415	946	34	980
	250	1593	82	1676	949	36	985
	300	1521	48	1569	1047	17	1064
	350	1608	57	1665	908	12	920
	400	1548	73	1621	1047	22	1069
	430	1562	68	1631	875	19	894

Table 3. Phytoplankton abundances analyzed microscopically in the GB and the LD, volume analyzed was 50 ml per sample.

		GB (cells mL^{-1})				LD (cells mL-1)			
		1 m	10 m	40 m	Total	1 m	10 m	40 m	Total
Cyanophyceae *	Total	14148	13536	0	27684	37368	32526	96	69990
Chryptophyta	Total	140	112	28	280	1400	882	56	2338
Bacillariophyceae	Total	96	94	44	234	462	112	102	676
	Chaetoceros sp.	58	42	24	124	434	106	26	566
	Skeletonema sp.	26	8	12	46	12	0	8	20
	Thalassiosira sp.	12	44	8	64	16	6	68	90
Dinophyceae	Total	3772	4424	1192	9388	9032	7662	1404	18098
	Dinophysis sp.	678	742	2	1422	450	214	4	668
	other	3094	3682	1190	7966	8582	7448	1400	17430
Chlorophyta	Total	5320	6860	28	12208	2072	1022	238	3332
	Planctonema sp.	5320	6860	28	12208	2072	1022	238	3332

* >90% were filamentous cyanobacteria *Aphanizomenon* sp.

Table 4. MnOx-like particles fluxes and size determined by image analysis in GB and LD.

Station	Depth (m)	MnOx-like particles ($cm^2\ m^{-2}d^{-1}$)	Median size ESD (μm)	Size range ESD (μm)
GB	110	5666.1± 993.5	2.8	0.6-166.7
	180	7789.1± 954.7	3.3	0.6-152.7
LD	110	50.3±1.8	1.8	0.6-16.5
	180	2.6±0.3	1.4	1.2-9.3

Table 5. Amino acids (AA), carbohydrates (CHO) and elemental molar ratios of sinking and suspended OM in the GB and in the LD.

	Depth (m)	AA-C:POC %	CHO-C:POC %	POC:PN	POC:POP	POC:Bsi	PN:POP
GB	40	19.19	18.26	9.80	244.05	3.86	0.39
sinking OM	40	17.58	17.21	9.43	222.42	4.07	0.43
	60	15.78	17.56	9.52	231.56	2.78	0.29
	110	13.87	22.24	11.31	90.12	1.73	0.15
	180	11.13	18.47	12.68	122.87	2.97	0.23
LD	40	13.52	9.43	12.17	771.70	3.58	0.29
sinking OM	40	14.27	8.40	11.09	413.14	4.12	0.37
	55	19.10	10.97	12.43	331.81	3.03	0.24
	110	13.37	11.97	15.44	229.70	2.67	0.17
	180	14.32	12.85	15.29	341.33	4.19	0.27
GB	1	8.22	16.94	10.39	154.56	91.45	14.88
suspended							
OM	10	10.81	8.84	10.48	150.51	87.15	14.36
	40	4.91	2.80	9.19	88.78	133.75	9.66
	60	5.43	2.66	9.78	127.36	125.24	13.02
	80	4.67		10.43	144.92		13.89
	110	9.01	6.63	8.45	245.26		29.01
	140	5.34		10.60	283.42		26.73
	180	5.73	4.29	11.37	506.21		44.54
	220	8.57	3.35	12.06	270.78		22.45
LD	1	6.96		8.66	205.29	514.94	23.71
suspended							
OM	10	12.97	9.12	8.43	196.44	100.91	23.31
	40	0.00	8.88	8.09	335.66	24.48	41.51
	60	6.09	10.26	7.83	300.75	16.89	38.43
	70	7.92	10.72	7.71	291.81	247.80	37.86
	110	12.22	5.41	7.93	224.56		28.32
	180	10.12	11.32	7.02	205.33		29.23
	250	11.97	8.81	6.52	249.36		38.22
	300	10.88		6.71	136.67		20.37
	350	10.67	10.12	6.76	145.80		21.56
	400	9.99		6.18	229.53		37.16
	430	9.35	9.45	7.82	148.61		19.01

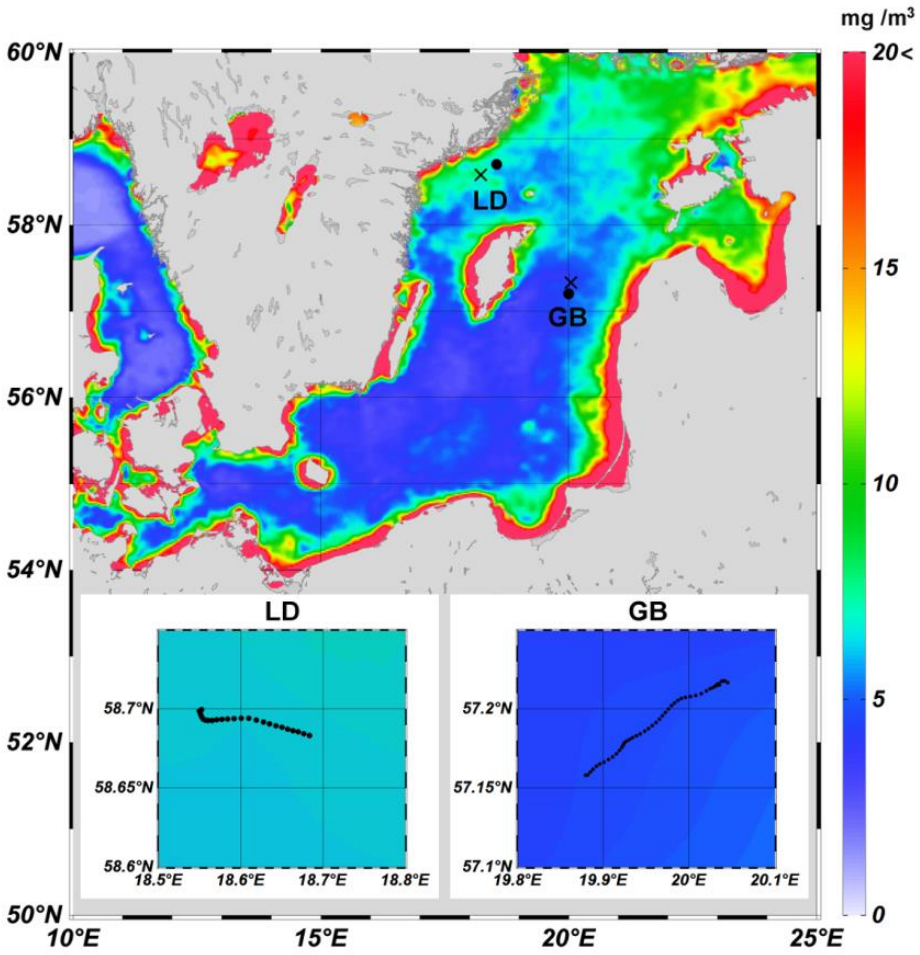
mg /m3
20<
15
10
5
0
60°N
58°N
56°N
54°N
52°N
50°N
10°E
15°E
20°E
25°E
LD
GB
LD
GB
58.7°N
58.65°N
58.6°N
18.5°E
18.6°E
18.7°E
18.8°E
57.2°N
57.15°N
57.1°N
19.8°E
19.9°E
20°E
20.1°E

Fig. 1

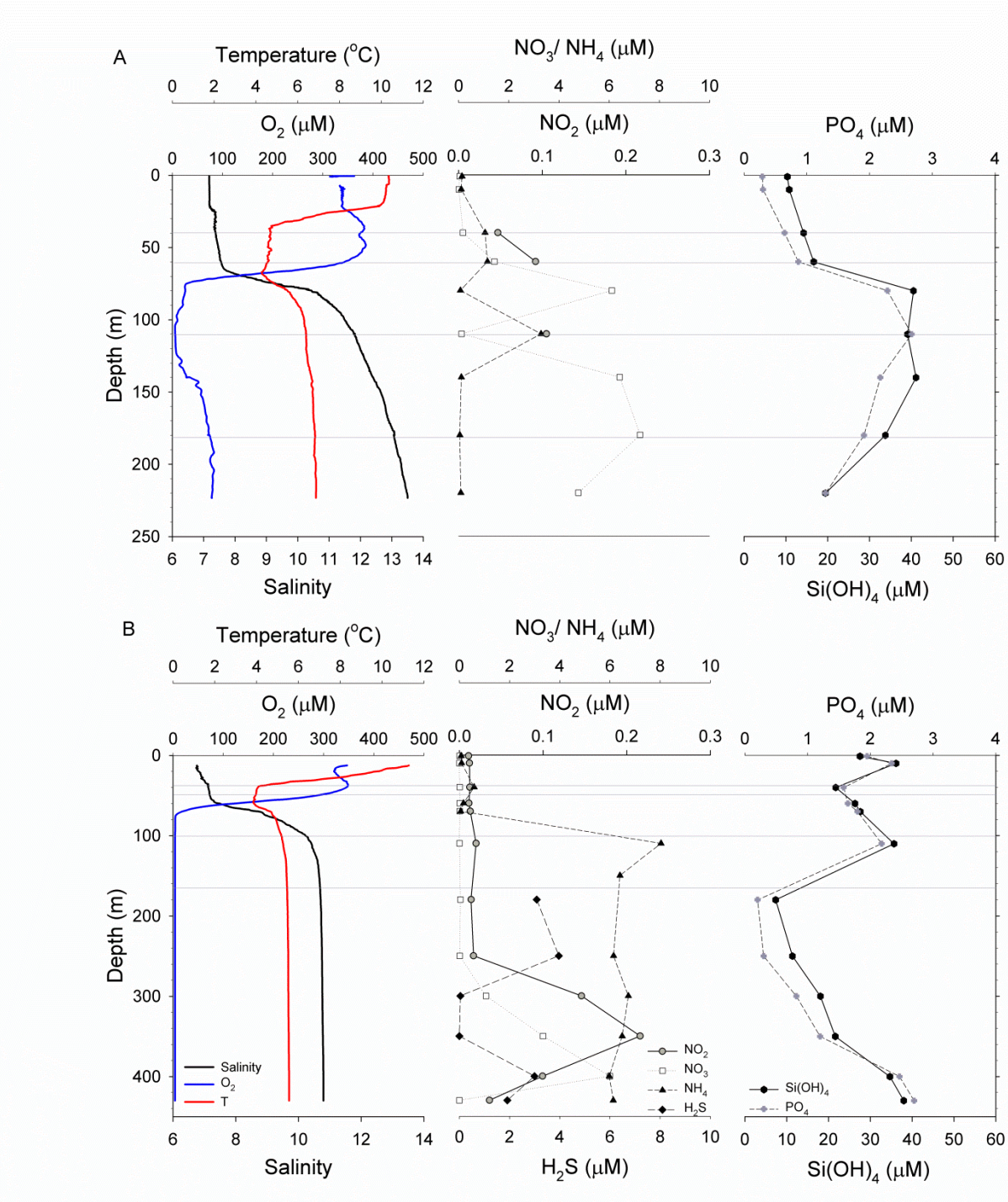
A
Temperature (°C)
NO_3/ NH_4 (μM)
O_2 (μM)
NO_2 (μM)
PO_4 (μM)
Depth (m)
Salinity
$Si(OH)_4$ (μM)
B
Temperature (°C)
NO_3/ NH_4 (μM)
O_2 (μM)
NO_2 (μM)
PO_4 (μM)
Depth (m)
Salinity
O_2
T
NO_2
NO_3
NH_4
H_2S
Si(OH)4
PO_4
Salinity
H_2S (μM)
$Si(OH)_4$ (μM)

Fig. 2

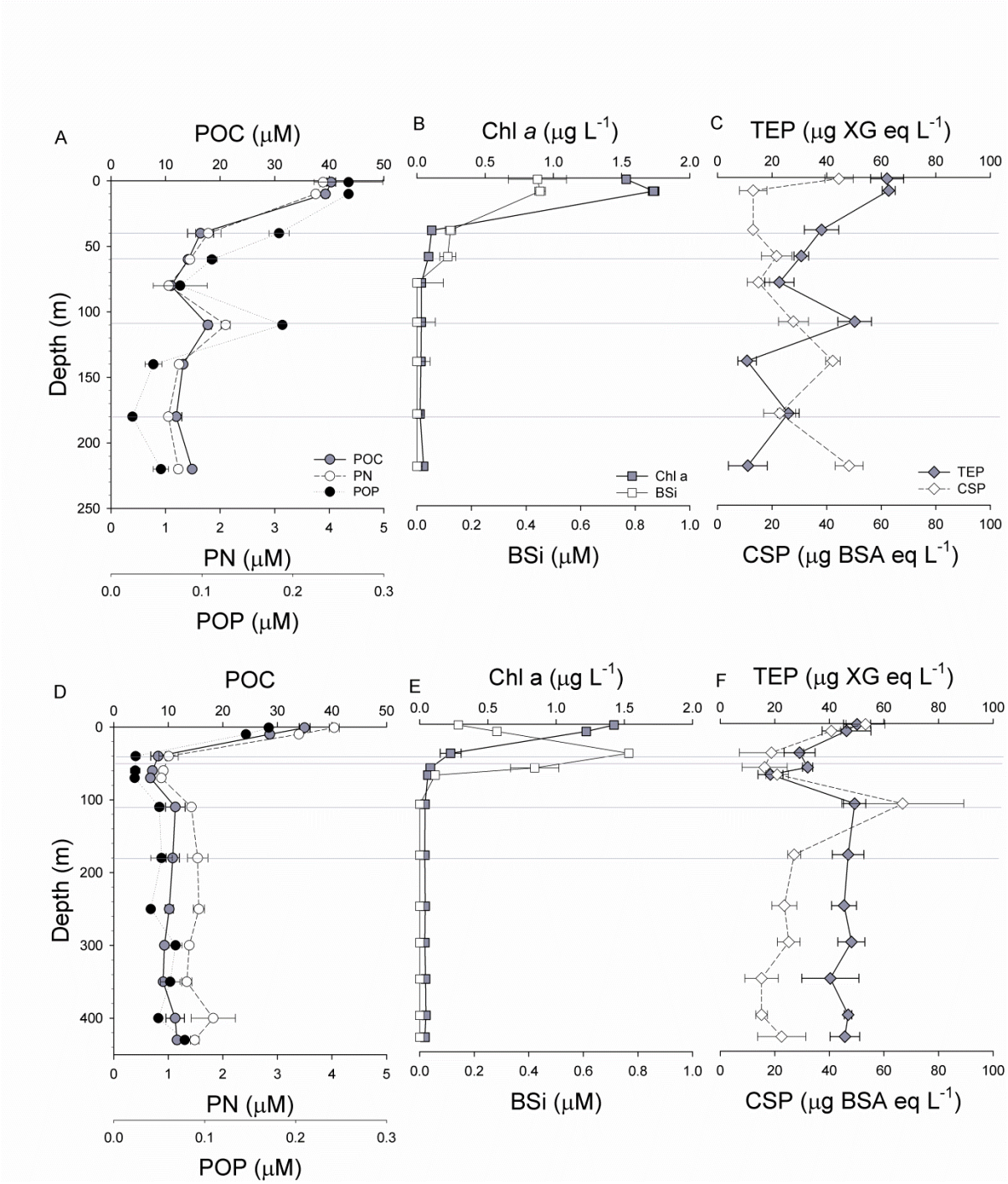
A
POC (μM)
B
Chl *a* (μg L^{-1})
C
TEP (μg XG eq L^{-1})
Depth (m)
POC
PN
POP
Chl a
BSi
TEP
CSP
PN (μM)
POP (μM)
BSi (μM)
CSP (μg BSA eq L^{-1})
D
POC
E
Chl a (μg L^{-1})
F
TEP (μg XG eq L^{-1})
Depth (m)
PN (μM)
POP (μM)
BSi (μM)
CSP (μg BSA eq L^{-1})

Fig. 3

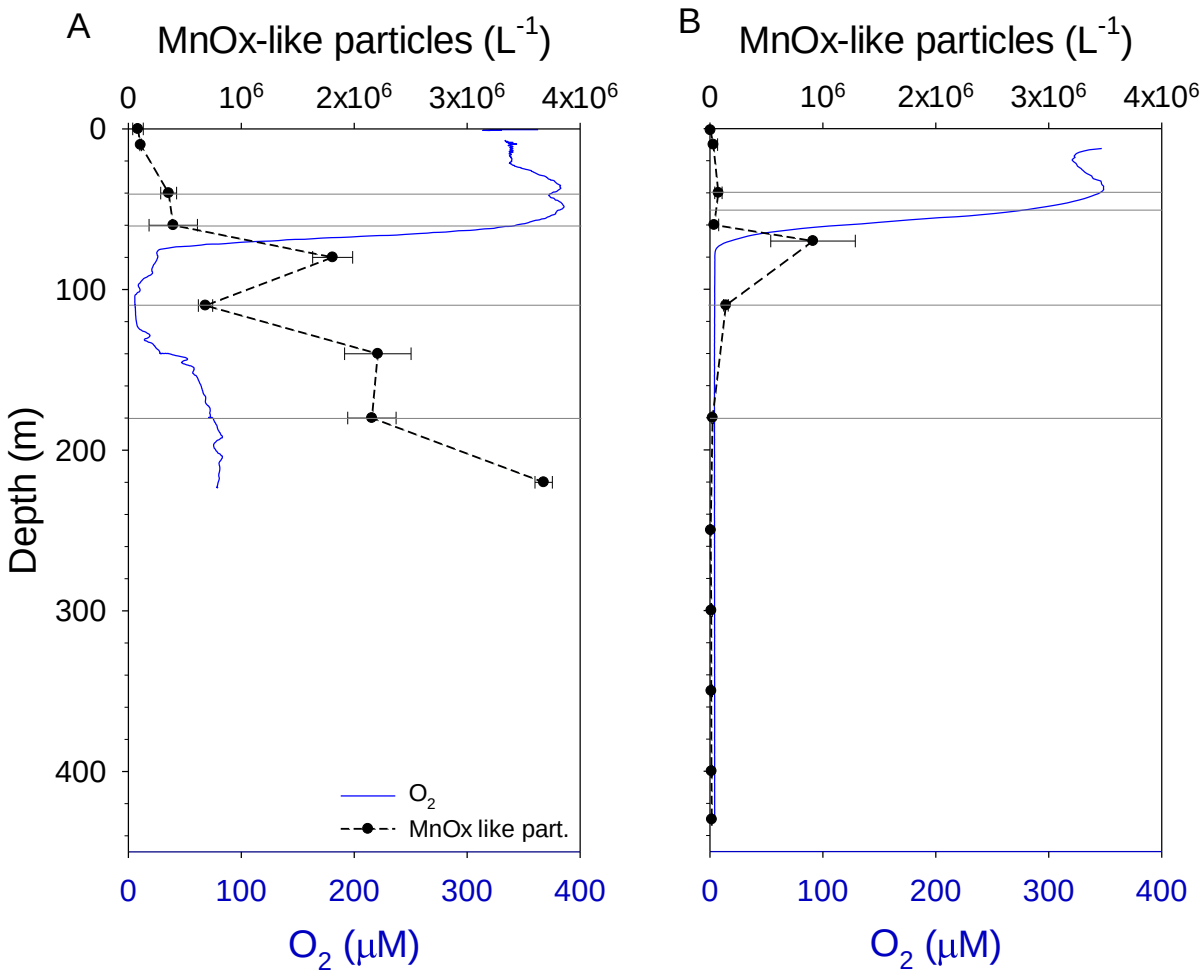
A
MnOx-like particles (L-1)
0
10^6
2x10^6
3x10^6
4x10^6
Depth (m)
0
100
200
300
400
O2
MnOx like part.
0
100
200
300
400
O2 (µM)
B
MnOx-like particles (L-1)
0
10^6
2x10^6
3x10^6
4x10^6
0
100
200
300
400
O2 (µM)

Fig. 4

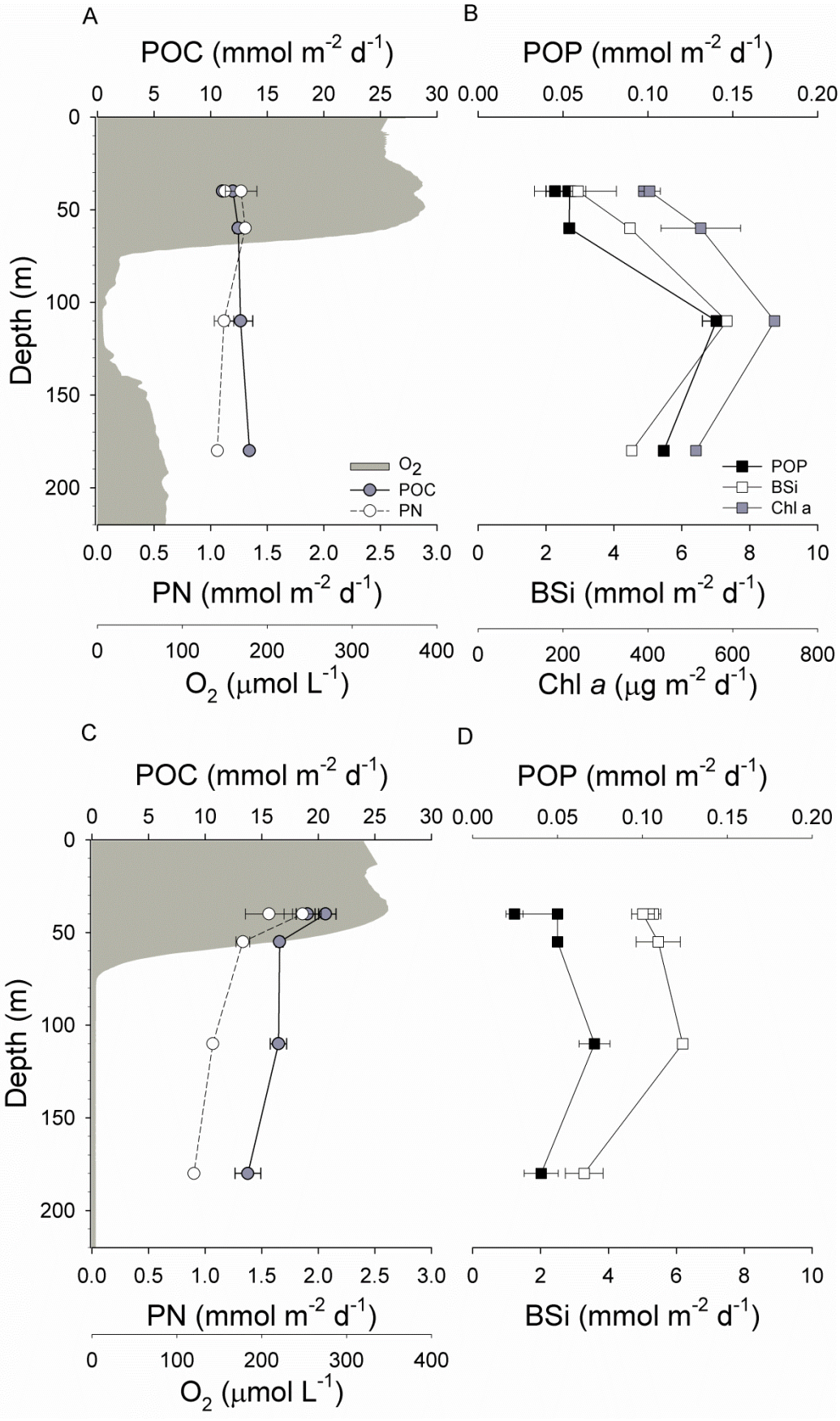
A
POC (mmol m-2 d-1)
0 5 10 15 20 25 30
Depth (m)
0 50 100 150 200
O2
POC
PN
0.0 0.5 1.0 1.5 2.0 2.5 3.0
PN (mmol m-2 d-1)
0 100 200 300 400
O2 (µmol L-1)
B
POP (mmol m-2 d-1)
0.00 0.05 0.10 0.15 0.20
POP
BSi
Chl a
0 2 4 6 8 10
BSi (mmol m-2 d-1)
0 200 400 600 800
Chl a (µg m-2 d-1)
C
POC (mmol m-2 d-1)
0 5 10 15 20 25 30
Depth (m)
0 50 100 150 200
0.0 0.5 1.0 1.5 2.0 2.5 3.0
PN (mmol m-2 d-1)
0 100 200 300 400
O2 (µmol L-1)
D
POP (mmol m-2 d-1)
0.00 0.05 0.10 0.15 0.20
0 2 4 6 8 10
BSi (mmol m-2 d-1)

Fig. 5

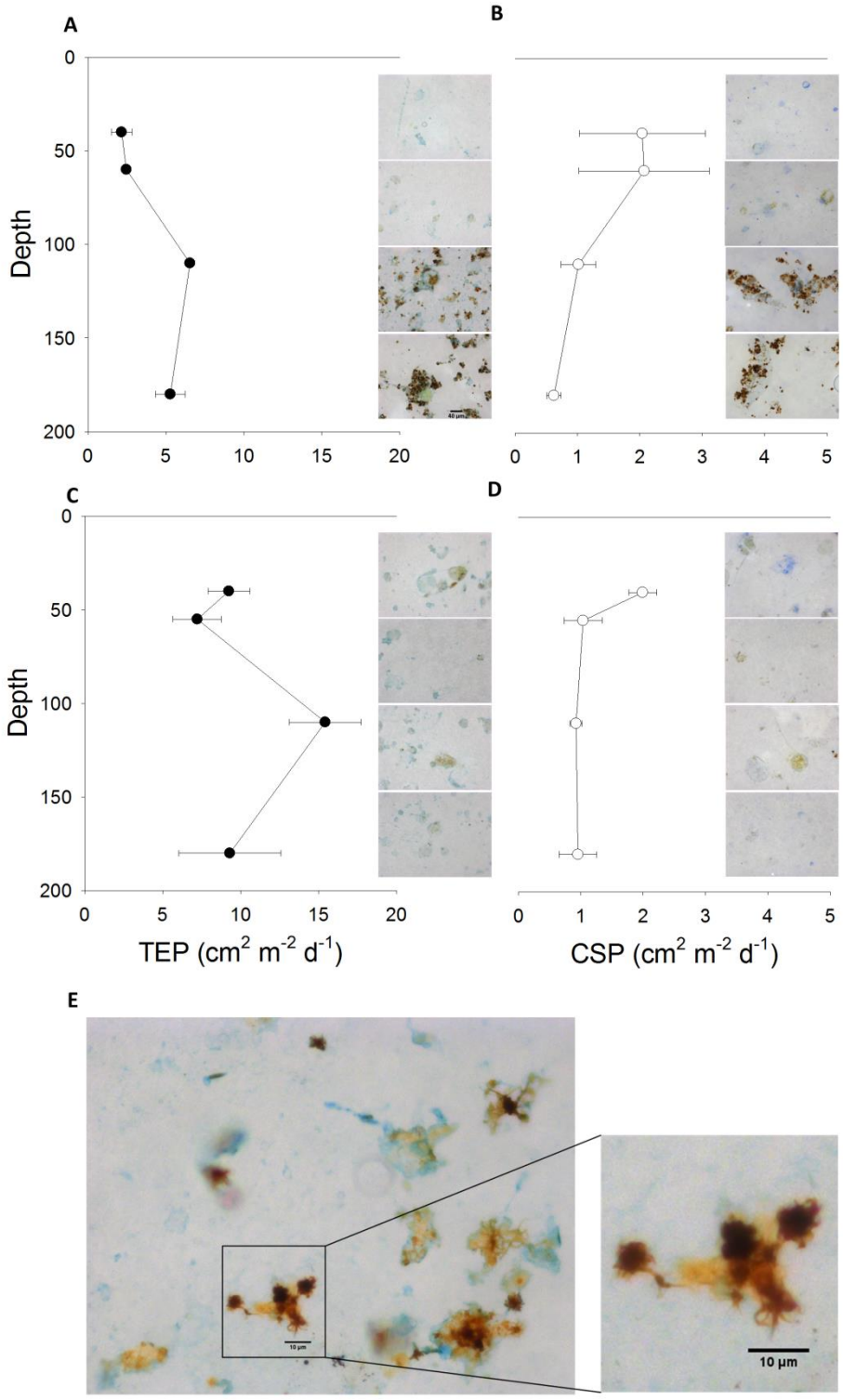
A
B
C
D
E
Depth
0
50
100
150
200
0
5
10
15
20
1
2
3
4
TEP (cm^2 m^{-2} d^{-1})
CSP (cm^2 m^{-2} d^{-1})
10 µm

Fig. 6

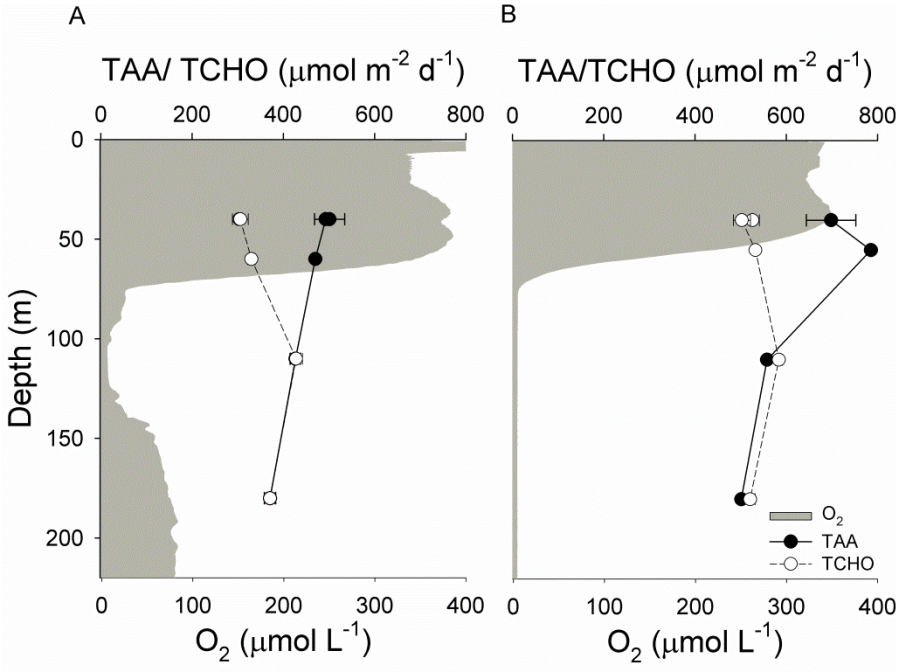
A
B
TAA/ TCHO (μmol m-2 d-1)
TAA/TCHO (μmol m-2 d-1)
0
200
400
600
800
Depth (m)
0
50
100
150
200
0
100
200
300
400
O2 (μmol L-1)
O2
TAA
TCHO

Fig. 7